Behavioral/Cognitive

Dopamine D_{2L} Receptor Deficiency Causes Stress Vulnerability through 5-HT_{1A} Receptor Dysfunction in Serotonergic Neurons

Norifumi Shioda,[1] Yoshiki Imai,[1] Yasushi Yabuki,[2] Wataru Sugimoto,[2] Kouya Yamaguchi,[2] Yanyan Wang,[3] Takatoshi Hikida,[4] Toshikuni Sasaoka,[5] Michihiro Mieda,[6] and Kohji Fukunaga[2]

[1]Department of Genomic Neurology, Institute of Molecular Embryology and Genetics, Kumamoto University, Kumamoto 860-0811, Japan, [2]Department of Pharmacology, Graduate School of Pharmaceutical Sciences, Tohoku University, Sendai 980-8578, Japan, [3]Department of Medical Information Science, College of Medicine, Carl R. Woese Institute for Genomic Biology, University of Illinois, Urbana, Illinois 61801, [4]Laboratory for Advanced Brain Functions, Institute for Protein Research, Osaka University, Osaka 565-0871, Japan, [5]Department of Comparative and Experimental Medicine, Brain Research Institute, Niigata University, Niigata 951-8585, Japan, and [6]Department of Integrative Neurophysiology, Graduate School of Medical Sciences, Kanazawa University, Kanazawa 920-8640, Japan

Mental disorders are caused by genetic and environmental factors. We here show that deficiency of an isoform of dopamine D_2 receptor (D_2R), $D_{2L}R$, causes stress vulnerability in mouse. This occurs through dysfunction of serotonin [5-hydroxytryptamine (5-HT)] 1A receptor (5-$HT_{1A}R$) on serotonergic neurons in the mouse brain. Exposure to forced swim stress significantly increased anxiety- and depressive-like behaviors in $D_{2L}R$ knock-out (KO) male mice compared with wild-type mice. Treatment with 8-OH-DPAT, a 5-$HT_{1A}R$ agonist, failed to alleviate the stress-induced behaviors in $D_{2L}R$-KO mice. In forced swim-stressed $D_{2L}R$-KO mice, 5-HT efflux in the medial prefrontal cortex was elevated and the expression of genes related to 5-HT levels was upregulated by the transcription factor PET1 in the dorsal raphe nucleus. Notably, $D_{2L}R$ formed a heteromer with 5-$HT_{1A}R$ in serotonergic neurons, thereby suppressing 5-$HT_{1A}R$-activated G-protein-activated inwardly rectifying potassium conductance in $D_{2L}R$-KO serotonergic neurons. Finally, $D_{2L}R$ overexpression in serotonergic neurons in the dorsal raphe nucleus alleviated stress vulnerability observed in $D_{2L}R$-KO mice. Together, we conclude that disruption of the negative feedback regulation by the $D_{2L}R$/5-HT_{1A} heteromer causes stress vulnerability.

Key words: **5-$HT_{1A}R$; D_2R; dopamine; mental disorders; serotonin; stress vulnerability**

Significance Statement

Etiologies of mental disorders are multifactorial, e.g., interactions between genetic and environmental factors. In this study, using a mouse model, we showed that genetic depletion of an isoform of dopamine D_2 receptor, $D_{2L}R$, causes stress vulnerability associated with dysfunction of serotonin 1A receptor, 5-$HT_{1A}R$ in serotonergic neurons. The $D_{2L}R$/5-$HT_{1A}R$ inhibitory G-protein-coupled heteromer may function as a negative feedback regulator to suppress psychosocial stress.

Introduction

Mental disorders, including anxiety and depression, have etiologies that are largely multifactorial, involving complex interactions between genetic and environmental factors (Caspi and Moffitt, 2006). Stress vulnerability in mental disorders has been linked to imbalances and/or dysfunctions of neurotransmitters, such as serotonin [5-hydroxytryptamine (5-HT)] and dopamine (DA), and variation in genes encoding proteins that impact the 5-HT and DA systems (Torres et al., 2003; Nutt, 2008; Caspi et al., 2010; Belujon and Grace, 2015; Grace, 2016). However, the direct interaction between 5-HT and DA receptors in psychological stress remains unclear.

Received Jan. 10, 2019; revised May 16, 2019; accepted May 28, 2019.

Author contributions: N.S. and K.F. designed research; N.S., Y.I., Y.Y., W.S., and K.Y. performed research; N.S., Y.Y., W.S., and K.Y. analyzed data; Y.W., T.H., T.S., and M.M. contributed unpublished reagents/analytic tools; N.S. and K.F. wrote the paper.

This work was supported by MEXT/JSPS KAKENHI (Grants 25460090 and 16K08265 to N.S.), KAKENHI (Grant 16H05219 to K.F.), the Takeda Science Foundation (N.S.), and partially supported by the Practical Research Project for Rare/Intractable Diseases from the Japan Agency for Medical Research and Development (AMED to N.S. and K.F.) and Grant-in Scientific Research on Innovation Areas "Constructive understanding of multiscale dynamism of neuropsychiatric disorders" (Grant 19H05221) from MEXT to N.S.

The authors declare no competing financial interests.

Correspondence should be addressed to Norifumi Shioda at shioda@kumamoto-u.ac.jp or Kohji Fukunaga kfukunaga@m.tohoku.ac.jp.

https://doi.org/10.1523/JNEUROSCI.0079-19.2019

Dysfunction of the 5-HT pathway in the brain contributes to the establishment of depression and anxiety disorders (Jans et al., 2007; Berger et al., 2009; Caspi et al., 2010; Booij et al., 2015). The diverse 5-HT receptors comprise seven main families (5-HT_1 to 5-HT_7), including at least 14 subtypes characterized by pharmacological-specific ligands, sequence diversity at gene and amino acid levels, and different second-messenger coupling systems (Hoyer et al., 2002). Among these, the 5-HT_{1A} receptor (5-$HT_{1A}R$) functions in the pathogenesis of anxiety and depression. For example, impaired binding potential of 5-$HT_{1A}R$ is associated with posttraumatic stress, panic disorders (Neumeister et al., 2004), and depression (Drevets et al., 1999). Promoter polymorphism in the 5-$HT_{1A}R$ gene (Lemonde et al., 2003) has been associated with anxiety-related personality traits (Strobel et al., 2003). Further, anxiety-like behaviors and stress responsiveness are elevated in mouse lacking the 5-$HT_{1A}R$ gene (Heisler et al., 1998; Parks et al., 1998; Ramboz et al., 1998).

Likewise, dysfunction of the DA pathway, especially the D_2 subtype of the dopamine receptor (D_2R), is related to anxiety and depression (Schneier et al., 2000; Lawford et al., 2006; Hayden et al., 2010; Sim et al., 2013). D_2R exists as two alternatively spliced isoforms, the D_2R long isoform ($D_{2L}R$) and the D_2R short isoform ($D_{2S}R$), which differ by a 29 aa insert in the intracellular third cytoplasmic loop (IC3; Dal Toso et al., 1989). In the mouse and primate brain, $D_{2L}R$ is more abundant, accounting for ~90% of the total D_2R expression, and predominates in the postsynaptic sites, whereas $D_{2S}R$ is less abundant and predominates in the presynaptic sites (Khan et al., 1998; Usiello et al., 2000; Wang et al., 2000; Lindgren et al., 2003). In human, frequent single nucleotide polymorphisms (rs2283265 and rs1076560) occur in introns 5 and 6, respectively, of the *DRD2* gene encoding D_2R; these polymorphisms independently alter transcriptional processing of exon 6, corresponding to the 29 aa insert (Zhang et al., 2007). Further, rs2283265 and rs1076560 reduce the $D_{2S}R$ mRNA levels relative to $D_{2L}R$ mRNA levels in the human striatum and prefrontal cortex (Zhang et al., 2007). In addition, these variants are associated with the development of schizophrenia (Bertolino et al., 2009). $D_{2L}R$ knock-out (KO) mouse displays age-related deficiency of the motor and learning functions (Fetsko et al., 2005), less exploration in hole board and zero maze test, and a higher increase in latency to escape from a foot-shock after the learned helplessness training compared with wild-type (WT) mice (Hranilovic et al., 2008). However, the involvement of $D_{2L}R$ abnormality in the onset of psychiatric disorders remains poorly understood.

To investigate whether genetic and environmental factors are critical for the expression of psychological characteristics, we examined anxiety- and depressive-like behaviors and their intracellular mechanisms in $D_{2L}R$-KO mice exposed to forced swim (FS) stress. We here report that $D_{2L}R$-KO mice exhibit stress vulnerability against FS stress via aberrant activation of serotonergic neurons. We also show that $D_{2L}R$ forms a heteromer with 5-$HT_{1A}R$ in serotonergic neurons, which is critical for 5-$HT_{1A}R$-induced inhibitory functions to suppress stress-related psychomotor behaviors.

Materials and Methods

Animals. In the current study, 10-week-old male C57BL/6J WT, homozygous $D_{2L}R$-KO (Wang et al., 2000), and D_2R-KO mice (Yamaguchi et al., 1996) were used. Mice were housed under climate-controlled conditions with a 12 h light/dark cycle, and provided standard food and water *ad libitum*. Animal studies were conducted in accordance with the Tohoku University institutional guidelines. Ethical approval has been obtained from the Institutional Animal Care and Use Committee of the Tohoku University Environmental and Safety Committee.

Cell culture and plasmid constructs. HEK293T cells (CRL-3216, American Type Culture Collection) were grown in DMEM (Sigma-Aldrich) supplemented with 10% heat-inactivated fetal bovine serum (FBS), 100 U/ml penicillin and 100 μg/ml streptomycin in a 5% CO_2 incubator at 37°C. Transfection was performed using Lipofectamine 2000 (Invitrogen) transfection reagent according to the manufacturer's protocol. The primary cultures of neurons were established using previously described methods, with slight modifications (Shioda et al., 2018). Briefly, the raphe nucleus tissue was dissected from embryonic day 18 mice, and dissociated by trypsin treatment and trituration through a Pasteur pipette. The neurons were plated on coverslips coated with poly-L-lysine in minimum essential medium (Invitrogen) supplemented with 10% FBS, 0.6% glucose (Wako), and 1 mM pyruvate (Sigma-Aldrich). After cell attachment, the coverslips were transferred to dishes containing a glial cell monolayer and maintained in neurobasal medium (Invitrogen) containing 2% B27 supplement (Invitrogen) and 1% GlutaMAX (Invitrogen). Further, 5 μM cytosine β-D-arabinofuranoside (Sigma-Aldrich) was added to cultures at 3 d *in vitro* (DIV) after plating, to inhibit glial proliferation. For whole-cell patch-clamp recording, primary cultured neurons at 21 DIV were used.

Plasmids encoding $D_{2L}R$-enhanced green fluorescent protein (EGFP), $D_{2S}R$-EGFP, and D_1R-EGFP were prepared as described previously (Shioda et al., 2017). Plasmids encoding HaloTag (HT)-5-$HT_{1A}R$ and adenosine A_{2A} receptor ($A_{2A}R$) were purchased from Promega. Plasmids encoding Venus-tagged $D_{2L}R$ and $D_{2S}R$, Rluc8-tagged 5-$HT_{1A}R$ and $A_{2A}R$ were generated using the KOD-Plus mutagenesis kit (Toyobo) according to the manufacturer's protocol. Finally, pAAV-IRES-GFP expression vector was purchased from Stratagene.

Behavioral analyses. In the open-field test, mice were placed in a Plexiglas box (30 × 30 × 30 cm) for 30 min, and their movements were recorded with a video camera. A circle with a 10 cm radius marked the center of the test floor, and time spent in that zone was recorded. This task is based on the mouse tendency to stay close to a wall in a state of high anxiety. In the during the open-field test, the locomotor activity was measured for 30 min using digital counters with an infrared sensor (DAS system, Neuroscience). In the elevated plus maze test, the task involved an apparatus consisting of a central 6 × 6 cm platform and four arms radiating like a plus sign from the platform: two open and two closed arms, all 30 cm long, 6 cm wide, and 10 cm high, with nontransparent sides and end walls. The maze was elevated 75 cm above the floor level. Mice were placed in the center facing the enclosed arm. The time spent in the enclosed arm was recorded. Prolonged periods in the enclosed arm are associated with increased anxiety behavior. In addition, the number of total arm entries was measured for evaluation of locomotor activity. In the tail-suspension test, the total duration of immobility induced by tail suspension was measured according to the method described by Shioda et al. (2010a). Briefly, acoustically and visually isolated mice were suspended 50 cm above the floor by an adhesive tape placed ~1 cm from the tip of the tail. Immobility time was recorded during a 5 min period. Mice were considered immobile only when they hung passively and remained completely motionless. In the FS test, mice were placed individually in glass cylinders (height: 25 cm, diameter: 16 cm) filled to the 20 cm level of water at 25°C, and the duration of immobility in a 6 min test was scored as described by Shioda et al. (2010a). Mice were judged immobile when they ceased to struggle and remained floating motionless in the water, making only those movements that were necessary to keep the head above the water. (±)-8-hydroxy-2-(dipropylamino)tetralin hydrobromide (8-OH-DPAT; Sigma-Aldrich; 0.1 or 1.0 mg/kg, i.p., in saline) or vehicle (saline) was administered to each mouse 30 min before the behavioral experiments.

Gene microarray analysis. To identify differentially expressed genes in the mouse dorsal raphe nucleus (DRN), we compared three FS-stressed mouse groups (WT, D_2R-KO, and $D_{2L}R$-KO) with non-stressed control WT group. The mice were subjected to 6 min of FS stress on 4 consecutive days, the DRN was dissected 12 h after the last FS stress exposure, and gene expression was analyzed. 3D-Gene Mouse Oligo Chip 24K arrays (Toray Industries) were used for oligo-DNA microarray analysis. Briefly,

total RNA was purified from the mouse DRN samples using RNeasy mini kit (Qiagen) according to the manufacturer's instructions. Total RNA was Cy5-labeled using the Amino Allyl Message AMP II aRNA amplification kit (Applied Biosystems). Labeled aRNA pools were then hybridized for 16 h using the supplier's protocols (http://www.3d-gene.com). Hybridization signals were scanned using a ScanArray express scanner (PerkinElmer) and processed using the GenePix Pro v5.0 software (Molecular Devices).

RT-qPCR. Total RNA was purified from the mouse DRN using the RNeasy mini kit (Qiagen) according to the manufacturer's protocol. RNA was then reverse-transcribed into single-stranded cDNA using an oligo(dT) primer (Promega) and Moloney murine leukemia virus reverse transcriptase (Invitrogen), and analyzed by reverse-transcription real-time quantitative PCR (RT-qPCR) with gene-specific primers. RT-qPCR analysis was performed as described previously (Shioda et al., 2018), in 48-well plates (Mini Opticon Real-Time PCR system, Bio-Rad) using iQ SYBR Green Supermix 2× (Bio-Rad). Gene expression was evaluated using the differences in normalized cycle threshold ($\Delta\Delta CT$) method after normalization to mouse *Gapdh* expression. FC in expression was calculated as $2^{-\Delta\Delta CT}$. The following primers were used: Tph2(FW) (5′-TCCTTTGACCCAAAGACGAC-3′); Tph2(RV) (5′-TTCAATGCTCTGCGTGTAGG-3′); Sert(FW) (5′-GGCTGAGATGAGGAACGAAG-3′); Sert(RV) (5′-CTATCCAAACCCAGCGTGAT-3′); Gchfr(FW) (5′-GGTGGGTGATGAACACTCG-3′); Gchfr(RV) (5′-GCTCATTCCTTGTGCAGACA-3′); Gapdh(FW) (5′-TGTGTCCGTCGTGGATCTGA-3′); and Gapdh(RV) (5′-ACCCAGAAGACTGRGGATGG-3′).

Immunoblotting. Immunoprecipitation and immunoblotting were performed as previously described (Shioda et al., 2018). The following primary antibodies were used: anti-TPH2 (1:500; Proteintech, 22590-1-AP), anti-D_2R (1:500; Millipore, AB1558), anti-5-HT_{1A}R (1:100; Santa Cruz Biotechnology, sc-1459), anti-PET1 (1:500; GeneTex, GTX51206), anti-SERT (1:500; Invitrogen, 702076), anti-GCHFR (1:500; Sigma-Aldrich, HPA046258), anti-β-tubulin (1:5000; clone AC-15, Sigma-Aldrich, A5441), and anti-GST (1:1000; Invitrogen, MA4-004) antibodies. The following secondary antibodies conjugated with horseradish peroxidase were used: anti-mouse IgG (1:5000; Southern Biotech, 1031-05), anti-rabbit IgG (1:5000; Southern Biotech, 4050-05), and anti-goat IgG (1:5000; Southern Biotech, 6420-05) antibodies. Immunoreactive bands were visualized using the luminescent image analyzer LAS-4000 (Fuji Film) and quantified using Image Gauge v3.41 (Fuji Film).

ChIP. Chromatin immunoprecipitation (ChIP) assay was performed as previously described (Shioda et al., 2018). Briefly, chromatin from tissues was prepared using the SimpleChIP plus enzymatic chromatin IP kit (Cell Signaling Technology) and then immunoprecipitated overnight at 4°C using 2 μg of anti-PET1 antibody (GeneTex, GTX51206). Assays included normal rabbit IgG as an antibody specificity control. The following primers were used: pTph2(FW) (5′-TTGGAAAAGTACAAATATAATCTT-3′); pTph2(RV) (5′-GCTTCCAAAACCCATGGTGTTTCC-3′); pSert(FW) (5′-AGGCAACCGGGCAGGAGGAGCAAG-3′); pSert(RV) (5′-TTTCAATGAACACACGTGTCTGCT-3′); pGchfr(FW) (5′-CGCGTCTCGCCTCGCCTCGTGCAC-3′); and pGchfr(RV) (5′-CTTCACTAGGAGTTGTGGCCATGG-3′).

Microdialysis experiment. Microdialysis experiments were performed as described previously (Shioda et al., 2010b). A guide cannula (AG-3, Eicom) was lowered into the medial prefrontal cortex (mPFC) 2 mm above the location of the probe tip, under anesthesia with 1.5% isoflurane. Mouse coordinates relative to the bregma were as follows (in mm): anterior = +1.9; lateral to the midline = +0.3; and down from the dura surface = −1.8. Following 24 h recovery, microdialysis probes (A-I-4-02, 2-mm-long dialysis membrane, outer diameter: 0.22 mm; Eicom) were inserted. Microdialysis was performed using a fully automated online system in HTEC-500ACA (Eicom) and HTEC-500GAA (Eicom) for 5-HT and DA analysis of FS-tested or freely moving mice. The microdialysis probe was perfused with Ringer's solution (in mm: 1.3 $CaCl_2$, 3 KCl, 146 NaCl, 1 $MgSO_4$) at a flow rate of 2.0 μl/min using a microsyringe pump (ESP-64, Eicom) throughout the experiment. KCl-induced 5-HT and DA concentrations were measured and averaged at the acute phase at a higher KCl concentration (1.3 mm $CaCl_2$, 146 mM KCl, 3 mM NaCl, and 1 mM $MgSO_4$) at a flow rate of 2.0 μl/min achieved using the microsyringe pump. Dialysates were collected every 6 min in the sample loop of an auto-injector (EAS-20, Eicom) and then analyzed using a high-performance liquid chromatography-electrochemical detector system (Eicom). For 8-OH-DPAT treatment, 8-OH-DPAT (0.1 mg per kg, i.p., in saline) or vehicle (saline) was administered 30 min before the microdialysis experiment.

Immunohistochemistry. Immunohistochemistry was performed as previously described (Shioda et al., 2018). The following primary antibodies were used: anti-TPH2 (1:250; Proteintech, 22590-1-AP), anti-D_2R (1:500; Millipore, AB1558), anti-5-HT_{1A}R (1:50; Santa Cruz Biotechnology, sc-1459), anti-HaloTag (1:500; Promega, G9281), and anti-GFP (1:1000; clone 9F9.F9, Abcam, ab1218) antibodies. The following secondary antibodies were used: AlexaFluor 488-conjugated donkey anti-rabbit (1:500; Invitrogen, A-21206), AlexaFluor 594-conjugated donkey anti-rabbit (1:500; Invitrogen, A-21207), AlexaFluor 488-conjugated donkey anti-mouse (1:500; Invitrogen, A-21202), AlexaFluor 594-conjugated donkey anti-mouse (1:500; Invitrogen, A-21203), AlexaFluor 488-conjugated donkey anti-goat (1:500; Invitrogen, A-11055), and AlexaFluor 594-conjugated donkey anti-goat (1:500; Invitrogen, A-11058) antibodies.

PLA. Proximity ligation *in situ* assay (PLA) was performed using mouse DRN slices fixed in 4% paraformaldehyde using the Duolink detection kit (Olink Bioscience) according to the manufacturer's instructions. To detect the interaction of D_2R with 5HT_{1A}R, the DRN slices were labeled with anti-goat Duolink PLA PLUS and anti-rabbit MINUS probes in a humidified oven at 37°C using goat anti-5HT_{1A}R antibody (1:50; Santa Cruz Biotechnology, sc-1459) and rabbit anti-D_2R antibody (1:500; Millipore, AB1558). In the assay, oligonucleotide tails of the secondary PLA PLUS and MINUS antibody probes hybridize when primary antibodies are in close proximity. Amplified end-products appear as green fluorescent spots in imaging, and each green spot represents an interaction between protein molecules.

Pull-down assay. D_2R-EGFP isoforms, D_1R-EGFP, and control EGFP proteins were affinity-purified using a GFP-nAb single-domain antibody system as specified in the manufacturer's protocols (ChromoTek). GST-5HT_{1A}R recombinant full-length protein was purchased from Abcam. Proteins binding to GST-5HT_{1A}R were prepared using a GST protein interaction pull-down kit (Pierce) according to the manufacturer's instructions. GST-5HT_{1A}R protein was immobilized on glutathione affinity resin. D_2R-EGFP isoforms, D_1R-EGFP, and control EGFP proteins were incubated with immobilized glutathione affinity resin containing GST-5HT_{1A}R protein at 4°C for 4 h with constant rotation. Subsequently, bound proteins were washed, eluted with glutathione elution buffer, and immunoblotted.

BRET assay. Bioluminescence resonance energy transfer (BRET) assay was performed as described previously (Shioda et al., 2017). Briefly, HEK293T cells were seeded on 10 cm plates and transfected with plasmids encoding Venus, D_{2L}R-Venus, D_{2S}R-Venus, 5-HT_{1A}R-Rluc8, or A_{2A}R-Rluc8. Then, 48 h after transfection, cells were harvested, washed, and suspended in PBS. Approximately 2×10^4 cells/well were placed in 96-well plates, and 5 μM coelenterazine H (Invitrogen) was added to each well. Fluorescence (excitation at 500 nm and emission at 540 nm) and luminescence were immediately quantified using a Flexstation3 multimode plate reader (Molecular Devices). The BRET signal was determined by calculating the ratio of light emitted by Venus (510–540 nm) to that emitted by Rluc8 (485 nm). The calculated Bmax and KD values using GraphPad Prism 7 (GraphPad Software) were taken as BRETmax and BRET50, respectively.

Preparation and injection of adeno-associated virus. To construct pAAV-Pet1/D_{2L}R-GFP, mouse D_{2L}R cDNA was subcloned downstream of the mouse *Pet1* promoter (Hasegawa et al., 2014) using pAAV-IRES-GFP expression vector (Stratagene). Plasmid pAAV-Pet1/GFP was used as a control construct. Viral particles were produced using the AAV2 helper-free system (Stratagene), according to the manufacturer's protocol, and titered by using an AAVpro titration kit (Takara Shuzo). For stereotaxic viral injections, the same titer (AAV-Pet1/D_{2L}R-GFP, 1.5×10^{12} genome copies/ml; AAV-Pet1/GFP, 1.7×10^{12} genome copies/ml) and equal amounts (1 μl) of viral particles were injected

into the DRN stereotaxically [at the following coordinates (in mm): anterior, −4.4; lateral, 0; ventral, −1.8] through a Hamilton syringe. Four weeks later, the mice were analyzed behaviorally, biochemically, and immunohistochemically.

Whole-cell patch-clamp recording. Experiments were performed as described previously (Muraki et al., 2004; Yabuki et al., 2017). Briefly, the external solution contained the following (in mM): 143 NaCl, 5 KCl, 2 $CaCl_2$, 1 $MgCl_2$, 10 glucose, and 10 HEPES (pH adjusted to 7.4 with NaOH, osmotic pressure 300–330 mOsm). Glass pipettes were filled with an internal solution containing the following (in mM): 70 potassium gluconate, 50 KCl, 26 NaCl, 3 $MgCl_2$, 0.5 $CaCl_2$, 2 ATP-Na_2, 10 EGTA, and 10 HEPES (pH adjusted to 7.4 with KOH, osmotic pressure 290–320 mOsm). The resistance of electrodes filled with the internal solution was 3.5–6.0 MΩ. To record the membrane potential, tetrodotoxin (100 nM) was included in the external solution to block the action potential induced by a voltage-gated sodium channel. 8-OH-DPAT (10, 30, and 60 μM), with or without Ba^{2+} (100 μM), was applied through the Y-tube (Yabuki et al., 2017). Cells were treated with AAV-Pet1/GFP or AAV-Pet1/D_{2L}R-GFP (10 μl each in culture medium) 7 d before the recordings. All current-clamp recordings were monitored at 25°C using an EPC10 single patch-clamp amplifier and acquisition system (HEKA), filtered at 3 kHz, and sampled at 10 kHz. The trace was analyzed using Patch Master (HEKA) and Igor Pro 6.05 (WaveMetrics) software.

Experimental design and statistical analysis. Comparisons between two experimental groups were made using a two-sided, unpaired Student's *t* test. Statistical significance for differences among groups was tested by one-way or two-way ANOVA with *post hoc* Bonferroni's multiple-comparison test. The value of $p < 0.05$ was considered significant. All statistical analyses were performed using GraphPad Prism 7. Microarray raw data are available at Gene Expression Omnibus; accession number GSE124806.

Results

D_{2L}R-KO mice show no responsiveness to 5-HT_{1A}R-mediated anti-anxiety and anti-depressive effects

WT, D_{2L}R-KO, and D_2R-KO mice were subjected to 6 min FS stress on 4 consecutive days (Days 0–3). Anxiety- and depressive-like behaviors of these mice were evaluated on Day 0 as a control, and on Days 1–3 after FS stress exposure (Fig. 1*A*). First, we analyzed the locomotor activity in the open-field test. In the test, the level of activity in the center of the open field is inversely related to the anxiety level. The WT mice spent significantly less time in the central area on Day 3 than on Day 0. This effect was even more pronounced in D_{2L}R-KO and D_2R-KO mice after FS stress on Days 1–3 (Fig. 1*B*, left; interaction: $F_{(6,132)} = 3.981$, $p = 0.0011$; Day: $F_{(3,132)} = 70.31$, $p < 0.0001$; Genotype: $F_{(2,132)} = 71.66$, $p < 0.0001$; $^{**}p < 0.01$, WT vs D_{2L}R-KO or D_2R-KO on each day; $\#\#p < 0.01$, Day 0 vs Day 3 in WT). As previously reported, D_2R in the basal ganglia is involved in the regulation of motor functions (Graybiel et al., 1994). Thus, we examined whether D_2R-KO and D_{2L}R-KO mice displayed any alterations in motor behavior. Total locomotor activity was significantly reduced in D_2R-KO compared with WT and D_{2L}R-KO mice. However, there was no difference in the total locomotor activity observed between WT and D_{2L}R-KO mice (Fig. 1*B*, right; interaction: $F_{(6,132)} = 0.279$, $p = 0.9460$; Day: $F_{(3,132)} = 16.84$, $p < 0.0001$; Genotype: $F_{(2,132)} = 211.1$, $p < 0.0001$; $^{**}p < 0.01$, WT or D_{2L}R-KO vs D_2R-KO on each day). Anxiety-like behavior was also evaluated using the elevated plus maze test. In all groups, exposure to FS stress significantly increased the time spent in the closed arms of the maze. Compared with WT mice, D_{2L}R-KO and D_2R-KO mice spent significantly more time in the closed arms on Days 1–3 (Fig. 1*C*, left; interaction: $F_{(6,132)} = 0.4646$, $p = 0.8335$; Day: $F_{(3,132)} = 68.57$, $p < 0.0001$; Genotype: $F_{(2,132)} = 40.12$, $p < 0.0001$; $^{**}p < 0.01$, $^{*}p < 0.05$, WT vs D_{2L}R-KO or D_2R-KO on each day, $\#\#p < 0.01$, Day 0 vs Days 1, 2, or 3 in WT). Consistent with results for of total locomotor activity in the open-field test, the number of total arm entries was significantly decreased in D_2R-KO compared with WT and D_{2L}R-KO mice. There was no difference in the number of total arm entries between WT and D_{2L}R-KO mice (Fig. 1*C*, right; interaction: $F_{(6,132)} = 0.1401$, $p = 0.9906$; Day: $F_{(3,132)} = 3.996$, $p = 0.0092$; Genotype: $F_{(2,132)} = 50.16$, $p < 0.0001$; $^{**}p < 0.01$, WT or D_{2L}R-KO vs D_2R-KO on each day). In the tail-suspension test evaluating depressive-like behavior, FS stress-induced increase in immobility time was more pronounced in D_{2L}R-KO and D_2R-KO mice than in WT mice on Days 2 and 3 (Fig. 1*D*; interaction: $F_{(6,132)} = 5.596$, $p < 0.0001$; Day: $F_{(3,132)} = 32.4$, $p < 0.0001$; Genotype: $F_{(2,132)} = 16.38$, $p < 0.0001$; $^{**}p < 0.01$, $^{*}p < 0.05$, WT vs D_{2L}R-KO or D_2R-KO on each day) Further, these mice were evaluated using the FS test. The FS stress induced significantly longer immobility time in D_{2L}R-KO and D_2R-KO mice than in WT mice on Days 1–3 (Fig. 1*E*; interaction: $F_{(6,132)} = 4.758$, $p = 0.0002$; Day: $F_{(3,132)} = 100.4$, $p < 0.0001$; Genotype: $F_{(2,132)} = 61.36$, $p < 0.0001$; $^{**}p < 0.01$, WT vs D_{2L}R-KO or D_2R-KO on each day; $\#\#p < 0.01$, Days 0 vs Day 3 in WT). These observations suggested that after FS stress exposure, the anxiety- and depressive-like behaviors in D_{2L}R-KO mice were more pronounced than in WT mice regardless of motor activity. On Day 3, these anxiety- and depressive-like behaviors were evaluated after pretreatment with the antidepressant 8-OH-DPAT, a selective 5-HT_{1A}R agonist. Although FS-stressed WT mice exhibited anti-anxiety and anti-depressive-like effects, D_{2L}R-KO mice showed no responsiveness to low-dose (0.1 mg/kg) and high-dose (1.0 mg/kg) 8-OH-DPAT in any behavioral test (Fig. 1*F*; open-field test, interaction: $F_{(2,54)} = 6.514$, $p = 0.0029$; Dose: $F_{(2,54)} = 14.49$, $p < 0.0001$; Genotype: $F_{(1,54)} = 138.3$, $p < 0.0001$; $^{**}p < 0.01$, vehicle vs 8-OH-DPAT in WT; $\#\#p < 0.01$, WT vs D_{2L}R-KO in 8-OH-DPAT; elevated plus maze test, interaction: $F_{(2,54)} = 1.378$, $p = 0.2608$; Dose: $F_{(2,54)} = 5.336$, $p = 0.0077$; Genotype: $F_{(1,54)} = 47.31$, $p < 0.0001$; $\#\#p < 0.01$, WT vs D_{2L}R-KO in 8-OH-DPAT: tail-suspension test, interaction: $F_{(2,54)} = 6.49$, $p = 0.0030$; Dose: $F_{(2,54)} = 16.08$, $p < 0.0001$; Genotype: $F_{(1,54)} = 107.5$, $p < 0.0001$; $^{**}p < 0.01$, vehicle vs 8-OH-DPAT in WT; $\#\#p < 0.01$, WT vs D_{2L}R-KO in 8-OH-DPAT: forced swim test, interaction: $F_{(2,54)} = 23.56$, $p < 0.0001$; Dose: $F_{(2,54)} = 47.01$, $p < 0.0001$; Genotype: $F_{(1,54)} = 290$, $p < 0.0001$; $^{**}p < 0.01$, vehicle vs 8-OH-DPAT in WT, $\#\#p < 0.01$, WT vs D_{2L}R-KO in 8-OH-DPAT).

D_{2L}R deficiency upregulates 5-HT homeostasis-related genes through PET1 activation in the DRN following FS stress

To explore the mechanism underpinning stress vulnerability and blunted 8-OH-DPAT effect in D_{2L}R-KO mice, we used DNA microarrays to analyze gene expression in the DRN. The DRN is the main source of widespread 5-HT projections to the forebrain, such as the mPFC, and 5-HT in the mPFC regulates the activity of neuronal circuits involved in such functions as emotional states and motivation (Celada et al., 2013). To identify differentially expressed genes, we compared three FS-stressed mouse groups (WT, D_2R-KO, and D_{2L}R-KO) with non-stressed control WT group. Gene expression was considered upregulated when the FC in expression was >3.0; it was considered to be downregulated when FC < 0.33. Among the 23,474 genes identified in the array, 397 genes were differentially expressed (44 upregulated and 353 downregulated) in FS-stressed WT mice compared with the unstressed WT group. In FS-stressed D_2R-KO group, 45 differentially expressed genes were identified (9 upregulated and 36 downregulated genes). In FS-stressed D_{2L}R-KO group, 36 differentially expressed genes were identified (7 upregulated and 29

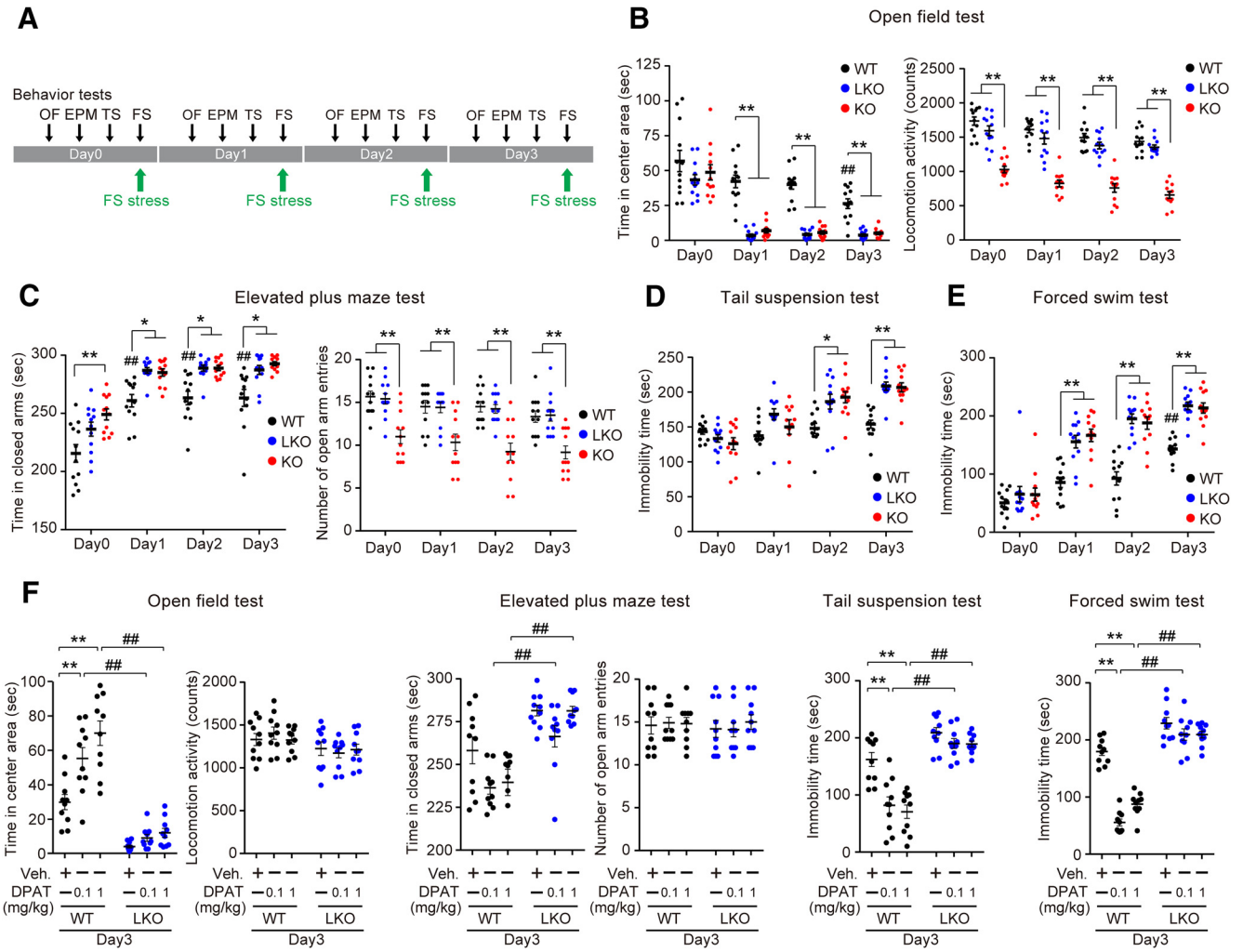

Figure 1. D_{2L}R-KO mice show no responsiveness to 5-HT_{1A}R-mediated anti-anxiety and anti-depressive effects. ***A***, Timelines of the sequence and duration of experimental protocols on anxiety- and depression-like behaviors in WT, D_{2L}R-KO, and D_2R-KO mice are shown. Mice were subjected to FS stress for 4 consecutive days (Days 0–3). The behaviors were assessed on Day 0 as a control, and on Days 1–3 after FS stress exposure. ***B–E***, D_{2L}R-KO and D_2R-KO mice show stress vulnerability to FS stress based on anxiety- and depression-related behaviors. Open-field test (left, time in center area; right, locomotor activity; ***B***), elevated plus maze test (left, time in closed arms; right, number of open arm entries; ***C***), tail-suspension test (***D***), and FS test (***E***) data are shown. $n = 12$ mice per group. ***F***, D_{2L}R-KO mice show no responsiveness to 8-OH-DPAT during behavioral tests; $n = 10$ mice per group. Data were presented as mean ± SEM and analyzed by two-way ANOVA with Bonferroni's *post hoc* test. [***B***, time in center area, $^{**}p < 0.01$, WT vs D_{2L}R-KO or D_2R-KO on each day; $^{\#\#}p < 0.01$, Day 0 vs Day 3 in WT; locomotor activity, $^{**}p < 0.01$, WT or D_{2L}R-KO vs D_2R-KO on each day]. [***C***, time in closed arms, $^{**}p < 0.01$, $^{*}p < 0.05$, WT vs D_{2L}R-KO or D_2R-KO on each day, $^{\#\#}p < 0.01$, Day 0 vs Day 1, 2 or 3 in WT; number of open arm entries, $^{**}p < 0.01$, WT or D_{2L}R-KO vs D_2R-KO on each day]. [***D***, $^{**}p < 0.01$, $^{*}p < 0.05$, WT vs D_{2L}R-KO or D_2R-KO on each day]. [***E***, $^{**}p < 0.01$, WT vs D_{2L}R-KO or D_2R-KO on each day; $^{\#\#}p < 0.01$, Days 0 vs Day 3 in WT]. [***F***, $^{**}p < 0.01$, vehicle vs 8-OH-DPAT in WT; $^{\#\#}p < 0.01$, WT vs D_{2L}R-KO in 8-OH-DPAT]. OF, open field test; EPM, elevated plus maze test; FS, forced swim test; TS, tail suspension test; DPAT, 8-OH-DPAT; WT, wild-type mice; LKO, D2LR-KO mice; KO, D2R-KO mice.

downregulated genes). Some of these differentially regulated genes overlapped in the stressed D_2R-KO and D_{2L}R-KO mice, but not with the stressed WT group (3 upregulated and 9 downregulated genes; Fig. 2*A*, top; microarray raw data are available at Gene Expression Omnibus, accession number GSE124806). Importantly, the overlapping subset of upregulated genes was related to 5-HT homeostasis. These were tryptophan hydroxylase 2 (*Tph2*), serotonin transporter (*Slc6a4*; also known as *Sert*), and GTP cyclohydrolase I feedback regulatory protein (*Gchfr*; Fig. 2*A*). We confirmed that the mRNA and protein levels of these three genes were significantly increased in the DRN of FS-stressed D_{2L}R-KO mice compared with non-stressed D_{2L}R-KO and FS-stressed WT mice [Fig. 2*B*; *Tph2*, interaction: $F_{(1,16)} = 26.05$, $p = 0.0001$; FS: $F_{(1,16)} = 8.265$, $p = 0.0110$; Genotype: $F_{(1,16)} = 15.57$, $p = 0.0012$. LKO vs FS+LKO ($t = 5.642$, $p = 0.0002$), FS+WT vs FS+LKO ($t = 6.399$, $p < 0.0001$); *Sert*, interaction: $F_{(1,16)} = 23.88$, $p = 0.0002$; FS: $F_{(1,16)} = 8.509$, $p = 0.0101$; Genotype: $F_{(1,16)} = 14.97$, $p = 0.0014$. LKO vs FS+LKO ($t = 5.518$, $p = 0.0003$), FS+WT vs FS+LKO ($t = 6.192$, $p < 0.0001$); *GCHFR*, interaction: $F_{(1,16)} = 13.06$, $p = 0.0023$; FS: $F_{(1,16)} = 3.777$, $p = 0.0698$; Genotype: $F_{(1,16)} = 9.431$, $p = 0.0073$. LKO vs FS+LKO ($t = 3.93$, $p = 0.0072$), FS+WT vs FS+LKO ($t = 4.727$, $p = 0.0014$) ; and Fig. 2*C* ; Tph2, $F_{(3,16)} = 36.83$, $p < 0.0001$, WT vs FS-LKO ($t = 8.519$, $p < 0.0001$), LKO vs FS-LKO ($t = 8.877$, $p < 0.0001$), FS-WT vs FS-LKO ($t = 8.314$, $p < 0.0001$); Sert, $F_{(3,16)} = 12.38$, $p = 0.0002$, WT vs FS-LKO ($t = 4.966$, $p = 0.0008$), LKO vs FS-LKO ($t = 5.277$, $p = 0.0005$), FS-WT vs FS-LKO ($t = 4.584$, $p = 0.0018$); Gchfr, $F_{(3,16)} = 14.58$, $p < 0.0001$, WT vs FS-LKO ($t = 5.298$, $p = 0.0004$), LKO vs FS-LKO ($t = 5.583$, $p = 0.0002$), FS-WT vs FS-LKO ($t = 5.3$, $p = 0.0004$)]. No differences in the 5-HT_{1A}R protein levels between the groups were noted (Fig. 2*C*).

PET1, an ETS domain transcription factor (human ortholog, FEV), is the only factor restricted to serotonergic neurons in the brain (Hendricks et al., 1999; Pfaar et al., 2002; Deneris and Wy-

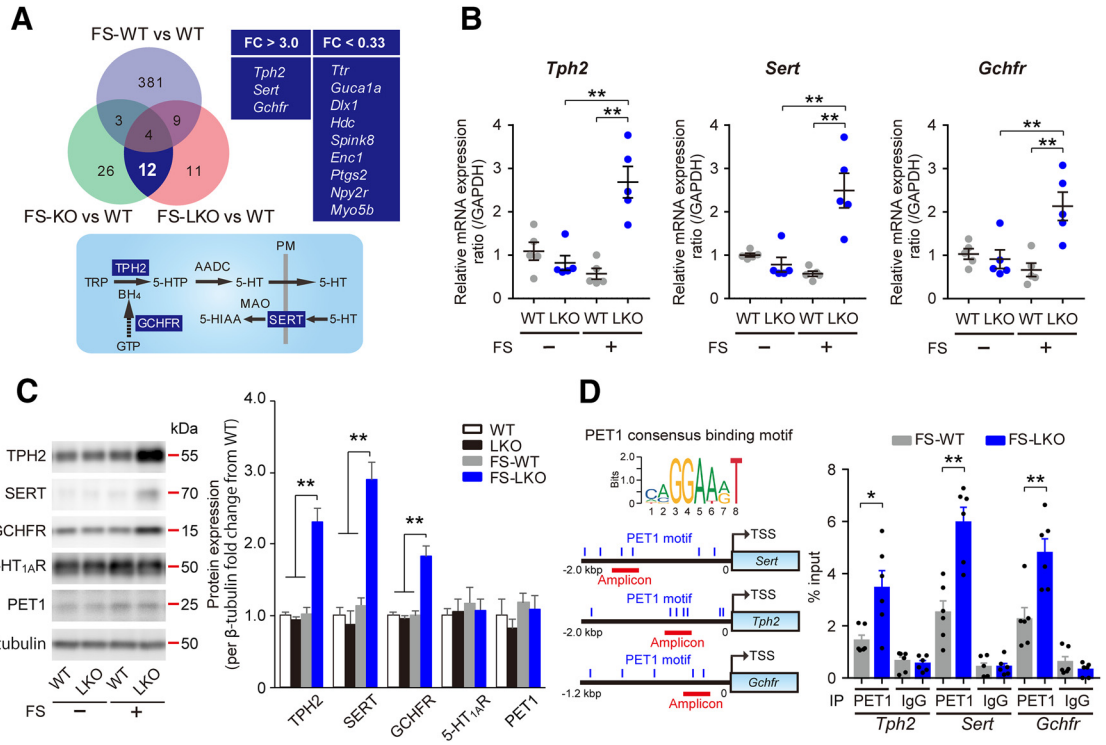

Figure 2. D_{2L}R deficiency upregulates the expression of 5-HT homeostasis-related genes through PET1 activation in the DRN following FS stress. ***A***, Top left, Venn diagram comparing gene expression in the DRN samples from FS-stressed animals from three groups (WT, D_2R-KO, and D_{2L}R-KO). FC in expression was compared with non-stressed control WT group (upregulated, FC > 3.0, and downregulated, FC < 0.33); $n = 5$ mice per group per pool. Top right, Three upregulated and nine downregulated genes overlapping in the FS-stressed D_2R-KO and D_{2L}R-KO groups, but not the FS-stressed WT group. Bottom, Serotonergic neurons express proteins related to 5-HT synthesis (TPH2, AADC, and GCHFR), reuptake (SERT), and metabolism (MAO). Tetrahydrobiopterin (BH_4), an essential cofactor of TPH2 for the synthesis of 5-HTP, is synthesized *de novo* from GTP. White letters surrounded by blue squares indicate the shared subsets of upregulated genes shown on the top right. ***B***, RT-qPCR analysis of mRNA levels in mouse DRN lysates. $n = 5$ mice each. Data were presented as mean ± SEM. $^{**}p < 0.01$ by two-way ANOVA with Bonferroni's *post hoc* test. ***C***, Left, Representative immunoblot of mouse DRN lysates probed with the indicated antibodies. Right, Densitometric analysis to determine the FC of indicated protein levels (normalized to β-tubulin) from WT. $n = 5$ mice each. Data were presented as means ± SEM. $^{**}p < 0.01$ by one-way ANOVA with Bonferroni's *post hoc* test. ***D***, Top left, Consensus binding motifs for the mammalian PET1 (Hendricks et al., 1999). Bottom left, PET1 motifs in promoter regions of the indicated genes. The motifs are indicated by blue vertical lines. Right, ChIP-qPCR analysis with a PET1 antibody and a negative control IgG using the indicated amplicons. Results are expressed as percentage input. Data are presented as mean ± SEM. $n = 6$ mice each. $^{**}p < 0.01$, $^{*}p < 0.05$ by two tailed unpaired *t* test. AADC, Aromatic l-amino acid decarboxylase; MAO, monoamine oxidase; 5-HIAA, 5-hydroxyindoleacetic acid; TRP, tryptophan; PM, plasma membrane; FS-WT, FS-stressed wild-type mice; LKO, D_{2L}R-KO mice; FS-LKO, FS-stressed D_{2L}R-KO mice; KO, D_2R-KO mice; FS-KO, FS-stressed D_2R-KO mice.

ler, 2012). PET1 coordinates gene expression of rate-limiting enzymatic (*Tph2*), 5-HT reuptake (*Sert*), and post-translational regulation (*Gchfr*), which determine the level of 5-HT synthesis in the mammalian brain (Deneris and Wyler, 2012; Wyler et al., 2015). In addition, *in vivo* ChIP and *in vitro* DNA binding assays demonstrated that PET1 coordinated the expression of these serotonergic genes by directly binding to a common ETS DNA binding site, with a conserved core consensus sequence [AGGAA(A/G)] identified in the promoter regions (Fig. 2*D*, left; Hendricks et al., 1999; Wei et al., 2010; Wyler et al., 2016). To determine whether PET1 targets ETS DNA binding sites of *Tph2*, *Sert*, and *Gchfr* following FS stress, we performed ChIP-qPCR of the DRN extracts with a PET1 antibody. We confirmed that the DRN samples from FS-stressed WT and D_{2L}R-KO mice contained equal levels of PET1 protein (Fig. 2*C*). A substantial PET1 enrichment at the promoter regions of *Tph2*, *Sert*, and *Gchfr* containing the ETS DNA binding site was revealed by ChIP analysis using primers targeting each amplicon in chromatin isolated from the DRN (Fig. 2*D*, left). Further, PET1 interaction with chromatin at this site was significantly more pronounced in FS-stressed D_{2L}R-KO mice than that in FS-stressed WT mice (Fig. 2*D*, right; Tph2: $t = 2.919$, DF = 10, $p = 0.0153$; Sert: $t = 4.731$, DF = 10, $p = 0.0008$; Gchfr: $t = 3.628$, DF = 10, $p = 0.0046$). Together, D_{2L}R deficiency is associated with an aberrant upregulation of 5-HT metabolism-related genes through PET1 in the DRN following stress stimulation.

FS stress-induced 5-HT efflux is elevated in the D_{2L}R-KO mPFC

To investigate changes in 5-HT efflux during FS stress, we used *in vivo* microdialysis in the mPFC of FS-stressed mice on Day 3. Although the basal 5-HT efflux in WT and D_{2L}R-KO mice was similar, FS stress-induced 5-HT efflux was markedly enhanced in the mPFC of D_{2L}R-KO mice compared with that in WT mice [Fig. 3*A*; WT vs LKO, interaction: $F_{(6,56)} = 5.062$, $p = 0.0003$; Time: $F_{(6,56)} = 13.95$, $p < 0.0001$; Genotype: $F_{(1,56)} = 21.33$, $p < 0.0001$, 12 min ($t = 5.947$, $p < 0.0001$), 18 min ($t = 3.858$, $p = 0.0021$)]. To confirm whether FS stress-induced 5-HT efflux in the mPFC is related to 5-HT_{1A}R, we measured 5-HT efflux following pretreatment with 8-OH-DPAT. As expected, the elevation of FS stress-induced 5-HT efflux was completely inhibited by 8-OH-DPAT in WT mice, but not in D_{2L}R-KO mice [Fig. 3*A*; WT: $F_{(6,28)} = 4.601$, $p = 0.0023$, 12 min ($t = 3.784$, $p = 0.0045$); LKO: $F_{(6,28)} = 10.32$, $p < 0.0001$, 12 min ($t = 5.662$, $p < 0.0001$), 18 min ($t = 3.54$, $p = 0.0085$); LKO+DPAT: $F_{(6,28)} = 19.99$, $p < 0.0001$, 12 min ($t = 7.783$, $p < 0.0001$), 18 min ($t = 4.931$, $p = 0.0002$)]. No significant change in FS stress-induced DA efflux was observed in the mPFC of WT or D_{2L}R-KO mice (Fig. 3*B*).

We further investigated whether D_{2L}R deficiency altered depolarization-induced 5-HT and DA efflux in the mPFC. A microdialysis probe was perfused with a high KCl solution to depolarize neurons in the mPFC of freely moving mice. After monitoring the basal 5-HT and DA efflux using normal Ringer's buffer, a high KCl-

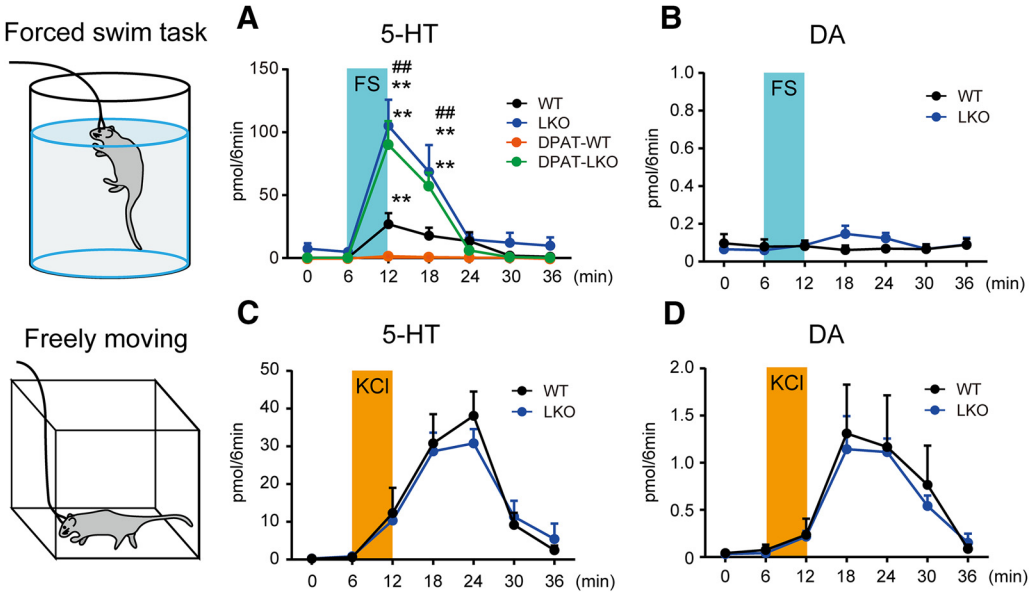

Figure 3. FS stress-induced 5-HT release is elevated in the D_{2L}R-KO mPFC. Extracellular 5-HT (***A***) and DA (***B***) concentrations in the mPFC in FS-stressed mice. Extracellular 5-HT (***C***) and DA (***D***) concentrations in the mPFC in freely moving mice; $n = 5$ mice each. Each bar represents the mean ± SEM. $^{**}p < 0.01$ by one-way ANOVA with Bonferroni's *post hoc* test. $^{\#\#}p < 0.01$ by two-way ANOVA with Bonferroni's *post hoc* test.

containing buffer was introduced into the microdialysis probe for 6 min. High KCl-induced 5-HT and DA effluxes were noted but were not significantly different in WT and D_{2L}R-KO mice (Fig. 3*C*,*D*). These observations suggested that excessive 5-HT efflux in the mPFC of D_{2L}R-KO mice depends largely on the excitability of projection neurons, not the local circuit neurons.

D_{2L}R forms a heteromer with 5-HT_{1A}R, and these proteins are expressed on serotonergic neurons

To determine D_2R and 5-HT_{1A}R localization in the DRN, we double-stained tissue sections using specific antibodies to these proteins and the serotonergic neuron marker TPH2. The anti-D_2R antibody used recognizes both D_2R isoforms. Strong 5-HT_{1A}R immunoreactivity was detected in TPH2-positive cells in the DRN of WT mice (Fig. 4*A*). D_2R was localized in both TPH2-positive (Fig. 4*B*) and 5-HT_{1A}R-positive (Fig. 4*C*, top) cells in the DRN of WT mice. Loss of immunoreactivity of the 5-HT_{1A}R-positive cells to the anti-D_2R antibody was observed in the DRN of D_{2L}R-KO mice (Fig. 4*C*, bottom), confirming specificity of the anti-D_2R antibody.

We also investigated the association between D_2R and 5-HT_{1A}R using antibodies against these proteins in conjunction with dual-recognition PLA. *In situ* PLA is used to test the interaction of two proteins localized at a distance <40 nm (Söderberg et al., 2006). We observed clear PLA signals, indicative of D_2R interaction with 5-HT_{1A}R in the WT DRN sections (Fig. 4*D*, left). By contrast, PLA signals indicative of the D_2R/5-HT_{1A}R interaction were undetectable in the D_{2L}R-KO DRN sections (Fig. 4*D*, right). We confirmed that the DRN lysates from D_{2L}R-KO mice contained significantly less D_2R protein than lysates from WT mice (Fig. 4*E*). To validate the direct binding of D_{2L}R and 5-HT_{1A}R, the interaction of purified EGFP-tagged D_2R isoforms, D_{2L}R-EGFP and D_{2S}R-EGFP, with recombinant GST-tagged 5-HT_{1A}R was analyzed by using the GST pull-down assay. In Western blot analysis with a GST antibody, we found that GST-5-HT_{1A}R directly bound to both EGFP-tagged D_2R isoforms, but not to EGFP and D_1R-EGFP used as negative controls (Fig. 4*F*). To confirm the specificity of the 5-HT_{1A}R antibody, we performed Western blot analysis with the antibody in these samples. GST-5-HT_{1A}R was also detected in samples of EGFP-tagged D_2R isoforms, but not EGFP and D_1R-EGFP. To confirm the interaction *in vivo*, we performed immunoprecipitation of DRN extracts with D_2R antibody followed by immunoblotting with 5-HT_{1A}R antibody. 5-HT_{1A}R signals were present in DRN extracts from WT mice but not from D_{2L}R-KO mice. Conversely, after 5-HT_{1A}R immunoprecipitation from DRN extracts, immunoblotting with D_2R antibody detected D_2R in brain extracts of WT but not D_{2L}R-KO mice (Fig. 4*F*).

We previously reported that D_{2S}R is expressed at the plasma membrane, and that D_{2L}R is located at the plasma membrane as well as intracellularly in EGFP-tagged D_2R isoforms overexpressing HEK293T cells and in mouse primary striatal neurons (Shioda et al., 2017). In the current study, we coexpressed EGFP-tagged D_2R isoforms and an HT-tagged 5-HT_{1A}R construct in HEK293T cells. As expected, D_{2L}R-EGFP and HT-5-HT_{1A}R co-localized at the plasma membrane and in the perinuclear region. In cells transfected with D_{2S}R-EGFP/HT-5-HT_{1A}R, these proteins were mainly detected on the plasma membrane (Fig. 4*G*). Next, we performed BRET assay to investigate heteromerization of D_2R isoforms and 5-HT_{1A}R in living cells. The transfer of energy between the bioluminescence donor Rluc8 luciferase and the fluorophore acceptor Venus occurs at a distance of $R_0 = 50$ Å, and no transfer is detected for distances >100 Å (Xu et al., 1999). BRET titration was performed in HEK293T cells for different construct combinations: Venus/5-HT_{1A}R-Rluc8, D_{2L}R-Venus/5-HT_{1A}R-Rluc8, D_{2S}R-Venus/5-HT_{1A}R-Rluc8, or D_{2L}R-Venus/A_{2A}-Rluc8. Significant BRET signal ratio, indicative of protein proximity, was detected for the D_{2L}R-Venus/5-HT_{1A}R-Rluc8 pair but not for the Venus/5-HT_{1A}R-Rluc8 pair, a negative control. An increase in BRET ratio was also observed for the D_{2S}R-Venus/5-HT_{1A}R-Rluc8 pair. D_{2L}R-Venus/A_{2A}R-Rluc8 pair was used as a positive control, as D_{2L}R was expected to specifically interact with A_{2A}R (Ciruela et al., 2004; Fig. 4*H*; BRETmax: 0.031 ± 0.01 for Venus/5-HT_{1A}R-Rluc8, 0.326 ± 0.07 for D_{2L}R-Venus/5-HT_{1A}R-Rluc8, 0.084 ± 0.03 for D_{2S}R-Venus/5-HT_{1A}R-Rluc8, and 0.217 ± 0.05 for D_{2L}R-Venus/A_{2A}R-Rluc8; BRET50:

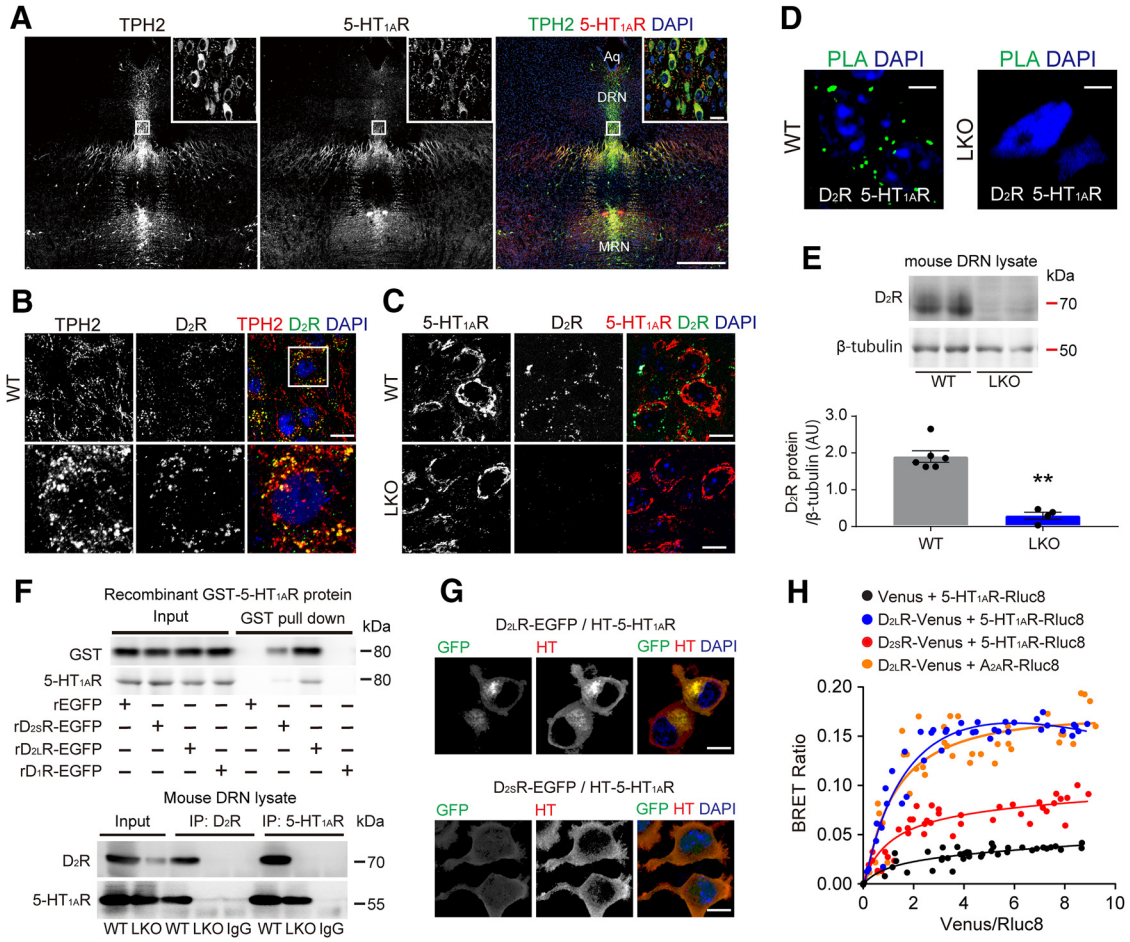

Figure 4. $D_{2L}R$ protein directly binds 5-$HT_{1A}R$ and colocalizes with it in serotonergic neurons. ***A–C***, Confocal images showing the localization of D_2R and TPH2 or 5-$HT_{1A}R$ in the DRN. TPH2 and 5-$HT_{1A}R$ immunoreactivities almost completely merge. MRN, Medial raphe nucleus; Aq, aqueduct. Scale bar, 400 μm. ***A***, D_2R colocalizes with both TPH2 (***B***) and 5-$HT_{1A}R$ (***C***) in the DRN. D_2R immunoreactivity is not detected in the D_2R-KO DRN samples (***C***, bottom). Boxed panels are high-magnification images of images in the white rectangles. Blue, DAPI. Scale bars, 10 μm. ***D***, D_2R association with 5-$HT_{1A}R$ as assessed by dual-recognition PLA. Signals indicative of the D_2R/5-$HT_{1A}R$ interaction are clearly seen in the WT DRN sections (left). D_2R/5-$HT_{1A}R$ interaction is undetectable in the $D_{2L}R$-KO DRN sections (right). PLA was repeated three times and representative data are shown. Blue, DAPI. Scale bars, 5 μm. ***E***, Top, Representative immunoblot of mouse DRN lysates probed with the indicated antibodies. Bottom, Densitometric analysis of D_2R levels normalized to β-tubulin (A.U., arbitrary units). WT, $n = 6$ mice; $D_{2L}R$-KO, $n = 4$ mice. Each bar represents the mean ± SEM. $^{**}p < 0.01$ by two tailed unpaired t test ($t = 7.628$, DF = 8, $p < 0.0001$). ***F***, Top, GST pull-down samples with purified recombinant (r)EGFP, EGFP-tagged rD_2R isoforms, or EGFP-tagged rD_1R with recombinant GST-5-$HT_{1A}R$ protein immunoblotted with GST antibody. Pull-down assay was repeated two times and representative data are shown. Bottom, Mouse DRN lysates were immunoprecipitated (IP) with the indicated antibodies and Western blots were probed with the indicated antibodies. ***G***, Confocal images showing colocalization of EGFP-tagged D_2R isoforms with Halo-tagged 5-$HT_{1A}R$. Blue, DAPI. Scale bars, 10 μm. ***H***, BRET saturation curves for the indicated receptor complexes. The fluorescence signal from Venus normalized to the luminescence of Rluc8 is shown on the x-axis. Each bar represents the mean ± SEM.

0.11 ± 0.12 for Venus/5-$HT_{1A}R$-Rluc8, 0.23 ± 0.09 for $D_{2L}R$-Venus/5-$HT_{1A}R$-Rluc8, 0.17 ± 0.1 for $D_{2S}R$-Venus/5-$HT_{1A}R$-Rluc8, and 0.22 ± 0.07 for $D_{2L}R$-Venus/$A_{2A}R$-Rluc8).

$D_{2L}R$ positively regulates 5-$HT_{1A}R$-mediated activity of the GIRK channel

G-protein-coupled inwardly rectifying potassium (GIRK) channels are the main effectors of 5-$HT_{1A}R$ (Williams et al., 1988), and they can be used as molecular targets for the study of depression and antidepressant responses involving the 5-$HT_{1A}R$-mediated signaling. Accordingly, we measured inward rectification of the GIRK channel-mediated hyperpolarization using a whole-cell voltage-clamp experiment in primary serotonergic neurons, identified in living cultured cells using AAV-Pet1/GFP (Fig. 5*A*). As expected, 8-OH-DPAT caused concentration-dependent hyperpolarization and pretreatment with a GIRK channel inhibitor Ba^{2+} significantly blocked 8-OH-DPAT-induced hyperpolarization [Fig. 5*B*; $F_{(3,15)} = 7.54$, $p = 0.0026$, DPAT-10 vs DPAT-30 ($t = 3.229$, $p = 0.0337$); DPAT-30 vs DPAT-30 + Ba^{2+} ($t = 3.733$, $p = 0.012$)]. To demonstrate that $D_{2L}R$ is functionally involved in the 5-$HT_{1A}R$-mediated GIRK signaling, we investigated 8-OH-DPAT-induced hyperpolarization in cultured serotonergic neurons from $D_{2L}R$-KO mice (Fig. 5*C*). In the presence of 8-OH-DPAT, the hyperpolarization response of the $D_{2L}R$-KO neurons was significantly lower than that of the WT neurons. Furthermore, expression of $D_{2L}R$ in the $D_{2L}R$-KO neurons from AAV-Pet1/$D_{2L}R$-GFP significantly rescued the hyperpolarization defect in these neurons [Fig. 5*D*; $F_{(2,15)} = 7.115$, $p = 0.0067$, WT vs LKO ($t = 3.558$, $p = 0.0086$); LKO vs LKO+$D_{2L}R$ ($t = 2.865$, $p = 0.0354$)].

$D_{2L}R$ expression in serotonergic neurons of the DRN reduces stress vulnerability in $D_{2L}R$-KO mice

To confirm that $D_{2L}R$ deficiency in the DRN led to stress vulnerability, we examined whether increasing $D_{2L}R$ protein levels in serotonergic neurons of the DRN rescued FS stress-induced behavioral alterations in $D_{2L}R$-KO mice. We injected adeno-associated virus (AAV; either AAV-Pet1/$D_{2L}R$-GFP or AAV-

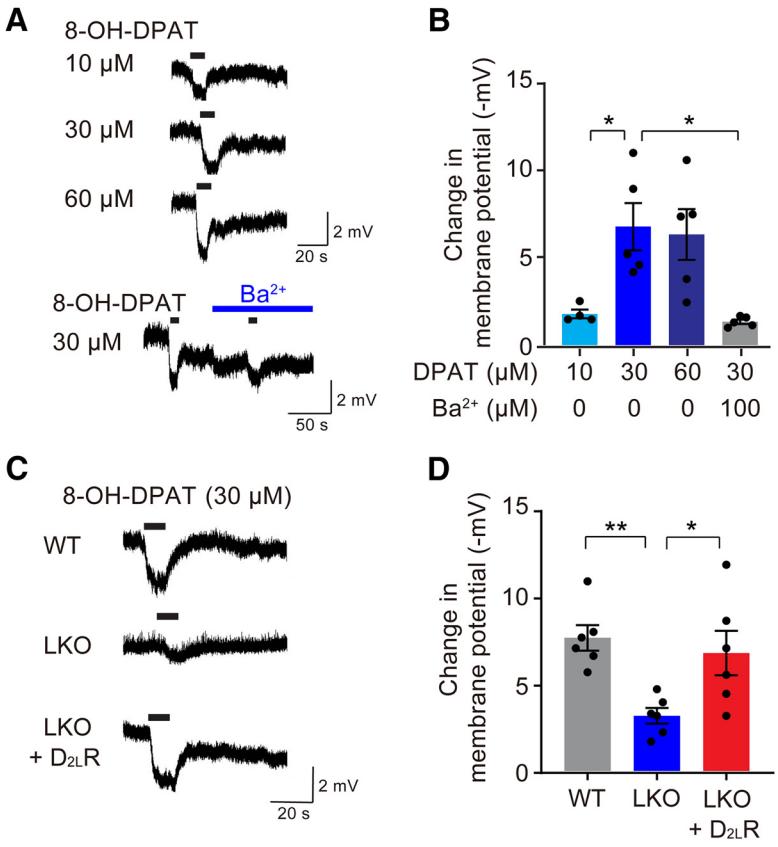

Figure 5. $D_{2L}R$ positively regulates 5-$HT_{1A}R$-mediated GIRK channel activity. ***A***, Representative traces of 8-OH-DPAT-induced (10, 30, and 60 μM) hyperpolarization, with or without Ba^{2+} (100 μM). Black bars indicate 8-OH-DPAT application (10 s). ***B***, GIRK channel inhibitor Ba^{2+} (100 μM) antagonizes 8-OH-DPAT-induced (30 μM) hyperpolarization. $n = 4–5$ cells per group. Each bar represents the mean ± SEM. *$p < 0.05$ by one-way ANOVA with Bonferroni's *post hoc* test. ***C***, Representative traces of 8-OH-DPAT-induced (30 μM) hyperpolarization in a primary serotonergic neuron derived from the WT and $D_{2L}R$-KO dorsal raphe upon $D_{2L}R$ overexpression. Black bars indicate 8-OH-DPAT application (10 s). ***D***, Overexpression of $D_{2L}R$ rescues attenuated 8-OH-DPAT-induced (30 μM) hyperpolarization in a $D_{2L}R$-KO serotonergic neuron. $n = 6$ per group. Each bar represents the mean ± SEM. **$p < 0.01$, *$p < 0.05$ by one-way ANOVA with Bonferroni's *post hoc* test.

Pet1/GFP, as a control) into the DRN of $D_{2L}R$-KO mice by stereotaxic surgery. Four weeks after the injection, the majority of GFP-positive infected cells in the DRN of each group were TPH2-positive serotonergic neurons (AAV-Pet1/GFP: 94.4 ± 1.8%; AAV-Pet1/$D_{2L}R$-GFP: 91.7 ± 2.4%; $n = 6$ mice; Fig. 6*A*, left). In addition, based on total D_2R levels, we confirmed that D_2R decrease in $D_{2L}R$-KO mice was significantly rescued in AAV-Pet1/$D_{2L}R$-GFP-treated $D_{2L}R$-KO mice [Fig. 6*A*, right; $F_{(2,6)} = 38.22$, $p = 0.0004$, WT-Veh vs LKO-Veh ($t = 7.685$, $p = 0.0008$); LKO-Veh vs LKO-D_2R ($t = 7.454$, $p = 0.0009$)].

Next, we investigated whether FS stress-induced increase of the expression of 5-HT metabolism-related genes *Sert*, *Tph2*, and *Gchfr* in the $D_{2L}R$-KO DRN was restored following AAV-Pet1/$D_{2L}R$-GFP treatment. Four weeks after the AAV injection in the DRN, the mice were subjected to 6 min FS stress on 4 consecutive days. The mRNA levels of the target genes in the FS-stressed $D_{2L}R$-KO DRN were all significantly reduced in the AAV-Pet1/$D_{2L}R$-GFP group compared with the AAV-Pet1/GFP group [Fig. 6*B*; *Tph2*, interaction: $F_{(1,20)} = 6.064$, $p = 0.0230$; FS stress: $F_{(1,20)} = 15.04$, $p = 0.0009$; Treatment: $F_{(1,20)} = 10.46$, $p = 0.0042$, LKO vs FS-LKO ($t = 4.483$, $p = 0.0014$), FS-LKO vs FS-LKO + $D_{2L}R$ ($t = 4.029$, $p = 0.0039$); *Sert*, interaction: $F_{(1,20)} = 14.67$, $p = 0.0010$; FS stress: $F_{(1,20)} = 15.76$, $p = 0.0008$; Treatment: $F_{(1,20)} = 13.68$, $p = 0.0014$, LKO vs FS-LKO ($t = 5.515$, $p = 0.0001$), FS-LKO vs FS-LKO + $D_{2L}R$ ($t = 5.323$, $p = 0.0002$); *Gchfr*, interaction: $F_{(1,20)} = 14.74$, $p = 0.0010$; FS stress: $F_{(1,20)} = 11.32$, $p = 0.0031$; Treatment: $F_{(1,20)} = 19.04$, $p = 0.0003$, LKO vs FS-LKO ($t = 5.093$, $p = 0.0003$), FS-LKO vs FS-LKO + $D_{2L}R$ ($t = 5.8$, $p < 0.0001$)].

Finally, we investigated whether the expression of $D_{2L}R$ in the DRN ameliorated stress vulnerability observed in $D_{2L}R$-KO mice. We injected the AAVs stereotaxically into the DRN of $D_{2L}R$-KO mice. Four weeks later, the mice were subjected to 6 min FS stress on 4 consecutive days. Then, 12 h after the last FS stress exposure, their anxiety- and depressive-like behaviors were evaluated. In the open-field test, FS stress resulted in a significant reduction of time spent in the central area by mice that received AAV-Pet1/GFP; the time spent in the central area by mice treated with AAV-Pet1/$D_{2L}R$-GFP was significantly improved [Fig. 6*C*; interaction: $F_{(1,36)} = 3.333$, $p = 0.0762$; FS stress: $F_{(1,36)} = 43.55$, $p < 0.0001$; Treatment: $F_{(1,36)} = 5.465$, $p = 0.0251$, LKO vs FS-LKO ($t = 5.957$, $p < 0.0001$), FS-LKO vs FS-LKO+$D_{2L}R$ ($t = 2.944$, $p = 0.0339$)]. In addition, in the elevated plus maze test, the animals receiving AAV-Pet1/$D_{2L}R$-GFP spent significantly less time in the closed arms than vehicle-treated mice [Fig. 6*D*; interaction: $F_{(1,36)} = 0.9471$, $p = 0.3370$; FS stress: $F_{(1,36)} = 41.16$, $p < 0.0001$; Treatment: $F_{(1,36)} = 17.26$, $p = 0.0002$, LKO vs FS-LKO ($t = 5.225$, $p < 0.0001$), FS-LKO vs FS-LKO+$D_{2L}R$ ($t = 3.625$, $p = 0.0053$)]. In the depressive-like behavior tail suspension test and FS test, the FS stress-induced increase in immobility time in vehicle-treated mice was ameliorated in AAV-Pet1/$D_{2L}R$-GFP-treated mice [Fig. 6*E*; interaction: $F_{(1,36)} = 17.57$, $p = 0.0002$; FS stress: $F_{(1,36)} = 31.59$, $p < 0.0001$; Treatment: $F_{(1,36)} = 24.03$, $p < 0.0001$, LKO vs FS-LKO ($t = 6.938$, $p < 0.0001$), FS-LKO vs FS-LKO+$D_{2L}R$ ($t = 6.431$, $p < 0.0001$); and Fig. 6*F*; interaction: $F_{(1,36)} = 3.16$, $p = 0.0839$; FS stress: $F_{(1,36)} = 70.92$, $p < 0.0001$; Treatment: $F_{(1,36)} = 4.323$, $p = 0.0448$, LKO vs FS-LKO ($t = 7.212$, $p < 0.0001$), FS-LKO vs FS-LKO+$D_{2L}R$ ($t = 2.727$, $p = 0.0588$)]. Hence, the expression of $D_{2L}R$ in the DRN significantly recovered stress vulnerability in $D_{2L}R$-KO mice.

Discussion

In the current study, we observed that $D_{2L}R$ deficiency causes stress vulnerability and we defined one mechanism underlying this vulnerability. We observed that: (1) exposure to FS stress increased anxiety- and depressive-like behaviors in $D_{2L}R$-KO mice; (2) administration of 8-OH-DPAT ameliorated the FS-induced behavior in WT mice but not in $D_{2L}R$-KO mice; and (3) FS-induced 5-HT efflux in the mPFC of $D_{2L}R$-KO mice was significantly elevated compared with WT, and it was associated with upregulation of the 5-HT metabolism-related genes in the $D_{2L}R$-KO DRN. We also showed that 5-$HT_{1A}R$ and $D_{2L}R$ formed a heteromer in serotonergic neurons of the DRN, and that $D_{2L}R$ overexpression in the serotonergic neurons of DRN ameliorated

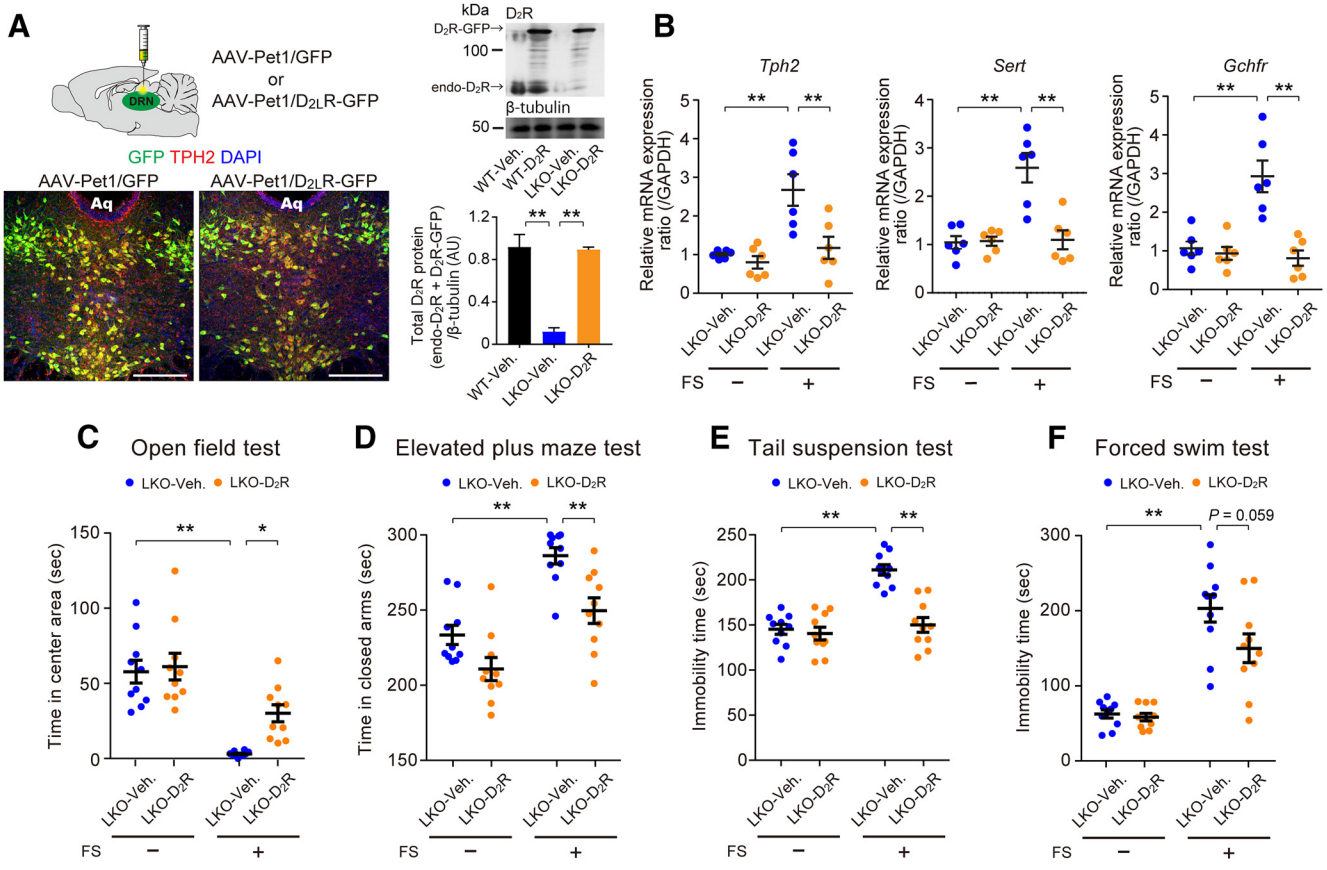

Figure 6. Overexpression of $D_{2L}R$ in 5-HT neurons of the DRN reduces stress vulnerability in $D_{2L}R$-KO mice. ***A***, Left, Representative immunofluorescence images showing AAV-Pet1/GFP (left) and AAV-Pet1/$D_{2L}R$-GFP (right) expression in the DRN. Green, GFP; red, TPH2; blue, DAPI; Aq, aqueduct. Scale bars, 250 μm. Right, Top, Representative immunoblot of mouse DRN lysates probed with the indicated antibodies. Bottom, Densitometric analysis of D_2R levels normalized to β-tubulin (A.U., arbitrary units). $^{**}p < 0.01$ by one-way ANOVA with Bonferroni's *post hoc* test. $n = 3$ mice each. endo-D_2R, Endogenous D_2R. ***B***, RT-qPCR analysis of mRNA levels in mouse DRN lysates. $n = 6$ mice each. Each bar represents the mean ± SEM. $^{**}p < 0.01$ by two-way ANOVA with Bonferroni's *post hoc* test. ***C–F***, Local expression of $D_{2L}R$ in the DRN ameliorates stress vulnerability in $D_{2L}R$-KO mice in the open-field test (***C***), elevated plus maze test (***D***), tail-suspension test (***E***), and FS test (***F***). $n = 10$ mice each. Each bar represents the mean ± SEM. $^{**}p < 0.01$, $^{*}p < 0.05$ by two-way ANOVA with Bonferroni's *post hoc* test.

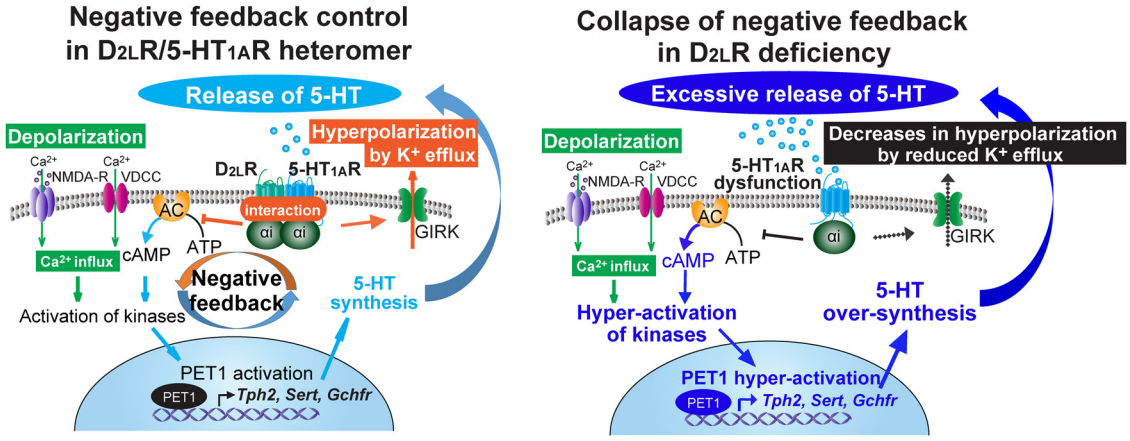

Figure 7. $D_{2L}R$ deficiency causes collapse of the negative feedback control of the $D_{2L}R$/5-$HT_{1A}R$ inhibitory G-protein-coupled heteromer in serotonergic neurons. (1) Stress-induced depolarization triggers Ca^{2+} influx through L-type voltage-dependent calcium channels (L-VDCC) and NMDA receptors (NMDA-R). (2) The Ca^{2+} influx leads to activation of numerous kinase pathways, resulting in activation of a transcription factor PET1, which is a key modulator of 5-HT synthesis. (3) PET1 activation increases *Tph2*, *Sert*, and *Gchfr* transcript levels, increasing 5-HT synthesis and extracellular release. (4) Extracellular 5-HT activates the $D_{2L}R$/5-$HT_{1A}R$ heteromer, and induces Gαi activation, inhibition of adenylyl cyclase (AC), and activation of GIRK currents. This results in decreased firing rate of serotonergic neurons and limits 5-HT release. In $D_{2L}R$ deficiency, 5-$HT_{1A}R$ cannot properly function against stress because of the collapse of the negative feedback mechanism, thereby eliciting excessive 5-HT release and stress vulnerability.

stress vulnerability. Together, the collapse of a negative feedback control of the $D_{2L}R$/5-HT_{1A} inhibitory G-protein-coupled heteromer in the DRN caused stress vulnerability, as shown in Figure 7.

We found that exposure to FS stress significantly increased anxiety- and depressive-like behaviors in both D_2R-KO and $D_{2L}R$-KO mice. In addition, to dissociate the role of locomotion from the anxiety- and depressive-like behaviors, we measured locomotor activity using open-field and elevated plus maze tests.

As reported previously (Usiello et al., 2000; Wang et al., 2000), D_2R-KO mice showed motor abnormalities in basal conditions, but $D_{2L}R$-KO mice did not (Fig. 1). Thus, among the two isoforms of D_2R, $D_{2L}R$ may be the genetic factor that contributes more to the vulnerability of stress-induced mental illness.

In support of the model of negative feedback regulation by the $D_{2L}R/5\text{-}HT_{1A}$ heteromer, $D_{2L}R$-KO mice exhibited reduced responsiveness to $5\text{-}HT_{1A}R$, with no apparent anti-anxiety and anti-depressive effects of the 8-OH-DPAT treatment (Fig. 1). Furthermore, upregulation of genes related to the expression of 5-HT, *Tph2*, *Sert*, and *Gchfr*, by PET1 (Deneris and Wyler, 2012; Wyler et al., 2015) was observed in the DRN (Figs. 2, 3). These findings explained the elevated FS-induced 5-HT efflux in the mPFC of $D_{2L}R$-KO mice. These observations suggested a dysfunction of $5\text{-}HT_{1A}R$ in $D_{2L}R$-KO mice. Consistent with these observations, dysfunction of $5\text{-}HT_{1A}R$ and 5-HT metabolism-related molecules are known to induce anxiety and depression behaviors in mice. For example, $5\text{-}HT_{1A}R$-KO mice display anxiety-like behaviors and elevated stress responsiveness (Heisler et al., 1998; Parks et al., 1998; Ramboz et al., 1998). Conversely, transgenic mice overexpressing $5\text{-}HT_{1A}R$ showed reduced anxiety-like behavior (Kusserow et al., 2004) and Tph2-KO mice showed reduced anxiety-like behavior in the open-field and elevated plus maze tests (Gutknecht et al., 2015).

Notably, $5\text{-}HT_{1A}R$ is expressed not only as an "autoreceptor" on serotonergic neurons in the midbrain raphe nuclei, which suppress the serotonergic tone as a negative feedback mechanism, but also as a "heteroreceptor", which enhances the postsynaptic inhibitory responses to 5-HT in the forebrain neurons receiving serotonergic innervation (Hamon et al., 1990; Beck et al., 1992; Riad et al., 2000). In this context, $5\text{-}HT_{1A}$ autoreceptor-KO mice showed increased anxiety (Richardson-Jones et al., 2010). On the other hand, $5\text{-}HT_{1A}$ heteroreceptor-KO mice showed largely unchanged anxiety levels, but enhanced depression-like behaviors and stress susceptibility (Richardson-Jones et al., 2011; Garcia-Garcia et al., 2017). In the current study, $D_{2L}R$ overexpression in serotonergic neurons of the DRN recovered the anxiety- and depressive-behaviors observed in $D_{2L}R$-KO mice (Fig. 6). Hence, we speculated that $D_{2L}R/5\text{-}HT_{1A}$ autoreceptors function to enhance the inhibitory G-protein-coupled receptor signaling. In the future, the relationship of the 5-HT raphe-forebrain circuit and $D_{2L}R/5\text{-}HT_{1A}R$ inhibitory G-protein-coupled heteromer in anxiety- and depressive-behaviors should be investigated.

In addition, activation of $5\text{-}HT_{1B}$ autoreceptor, which displays 43% amino-acid sequence homology with $5\text{-}HT_{1A}$ (Hoyer et al., 2002), decreases both the firing of the serotonergic neurons and 5-HT synthesis, thereby functioning as a negative feedback system to fine-tune synaptic 5-HT concentrations (Hoyer and Middlemiss, 1989; Hjorth et al., 1995). Although not clarified in the present study, it is worth exploring that $D_{2L}R$ might also form a heteromer with $5\text{-}HT_{1B}R$ in serotonergic neurons of the DRN and might have a suppressive role in the serotonergic tone as a negative feedback mechanism.

Although D_2R and $5\text{-}HT_{1A}R$ heteromer formation has been shown using Forster resonance energy transfer in HEK293 cells (Łukasiewicz et al., 2016), a direct interaction has not been evidenced *in situ*. Here, we showed that $D_{2L}R$ directly interacts with $5\text{-}HT_{1A}R$ *in vitro* and *in vivo* (Fig. 4). It has been proposed that D_2R exists as heteromeric complexes with other G-protein-coupled receptors, and that the heteromer forms between positively charged residues of IC3 of D_2R and negatively charged acidic residues in the other G-protein-coupled receptors (Fuxe et al., 2010; Borroto-Escuela and Fuxe, 2017). For example, the $D_2R/A_{2A}R$ heteromer is formed by electrostatic interactions between the IC3 D_2R residues ($_{217}$RRRRKR$_{222}$), which are present in both $D_{2L}R$ and $D_{2S}R$, and two adjacent aspartate residues ($_{401}$DD$_{402}$) in the C-terminal tail of $A_{2A}R$ (Ciruela et al., 2004). Similarly, the IC3 of D_2R interacts with adjacent glutamic acid residues in the C-terminal tail of the dopamine D_1R ($_{404}$EE$_{405}$; Łukasiewicz et al., 2009). Furthermore, the IC3 of D_2R interacts with the C-terminal tail of $5\text{-}HT_{2A}R$ ($_{454}$EE$_{455}$; Łukasiewicz et al., 2010). Whereas the C-terminal tail of $5\text{-}HT_{1A}R$ is short, the IC3 is long, consisting of 132 aa, with two adjacent aspartate residues ($_{285}$DD$_{286}$). Although we could not determine the exact residues critical for the $D_2R/5\text{-}HT_{1A}R$ interaction, electrostatic interactions between the positively charged IC3 D_2R residues and the negatively charged IC3 $5\text{-}HT_{1A}R$ residues may be envisaged. Interestingly, the 29 aa insert (G_{242}–V_{270}) in the IC3 seen only in $D_{2L}R$ contains an arginine-rich region ($_{267}$RRR$_{269}$), and we showed that $5\text{-}HT_{1A}R$ binds more strongly to $D_{2L}R$ than to $D_{2S}R$ (Fig. 4*H*). The exact binding residues of $D_{2L}R$ and $5\text{-}HT_{1A}R$ should be examined in detail in the future.

Both D_2R and $5\text{-}HT_{1A}R$ are well established targets for various pharmacological compounds and third-generation antipsychotics, such as aripiprazole and lurasidone. These compounds have affinity for both these receptors, and are used to manage positive symptoms by interactions with D_2R and to simultaneously manage negative symptoms by activating $5\text{-}HT_{1A}R$ (Newman-Tancredi and Kleven, 2011). Therefore, specific pharmacological profiling of the $D_{2L}R/5\text{-}HT_{1A}R$ heteromer may inform a novel therapeutic strategy. One approach based on the notion of receptor dimerization involves bivalent ligands, which are formed of two ligand moieties linked via a spacer, and capable of binding to both protomers of a dimer, such as D_2R/D_2R homodimers (Kühhorn et al., 2011) and $D_2R/A_{2A}R$ heterodimers (Soriano et al., 2009). The drug discovery research targeting the $D_2R/5\text{-}HT_{1A}R$ heteromer may be an attractive therapy for mental disorders.

In conclusion, we showed the cause of mental stress vulnerability associated with the $D_{2L}R$ abnormality in the mouse brain. $D_{2L}R$ and $5\text{-}HT_{1A}R$ form a heteromer in the DRN, and they are important for negative feedback control of the inhibitory G-protein-coupled signaling in serotonergic neurons against psychosocial stress.

References

Beck SG, Choi KC, List TJ (1992) Comparison of 5-hydroxytryptamine 1A-mediated hyperpolarization in CA1 and CA3 hippocampal pyramidal cells. J Pharmacol Exp Ther 263:350–359.

Belujon P, Grace AA (2015) Regulation of dopamine system responsivity and its adaptive and pathological response to stress. Proc Biol Sci 282: 20142516.

Berger M, Gray JA, Roth BL (2009) The expanded biology of serotonin. Annu Rev Med 60:355–366.

Bertolino A, Fazio L, Caforio G, Blasi G, Rampino A, Romano R, Di Giorgio A, Taurisano P, Papp A, Pinsonneault J, Wang D, Nardini M, Popolizio T, Sadee W (2009) Functional variants of the dopamine receptor D2 gene modulate prefronto-striatal phenotypes in schizophrenia. Brain 132:417–425.

Booij L, Tremblay RE, Szyf M, Benkelfat C (2015) Genetic and early environmental influences on the serotonin system: consequences for brain development and risk for psychopathology. J Psychiatry Neurosci 40:5–18.

Borroto-Escuela DO, Fuxe K (2017) Diversity and bias through dopamine D2R heteroreceptor complexes. Curr Opin Pharmacol 32:16–22.

Caspi A, Moffitt TE (2006) Gene–environment interactions in psychiatry: joining forces with neuroscience. Nat Rev Neurosci 7:583–590.

Caspi A, Hariri AR, Holmes A, Uher R, Moffitt TE (2010) Genetic sensitivity to the environment: the case of the serotonin transporter gene and its

implications for studying complex diseases and traits. Am J Psychiatry 167:509–527.

Celada P, Puig MV, Artigas F (2013) Serotonin modulation of cortical neurons and networks. Front Integr Neurosci 7:25.

Ciruela F, Burgueño J, Casadó V, Canals M, Marcellino D, Goldberg SR, Bader M, Fuxe K, Agnati LF, Lluis C, Franco R, Ferré S, Woods AS (2004) Combining mass spectrometry and pull-down techniques for the study of receptor heteromerization: direct epitope-epitope electrostatic interactions between adenosine A2A and dopamine D2 receptors. Anal Chem 76:5354–5363.

Dal Toso R, Sommer B, Ewert M, Herb A, Pritchett DB, Bach A, Shivers BD, Seeburg PH (1989) The dopamine D2 receptor: two molecular forms generated by alternative splicing. EMBO J 8:4025–4034.

Deneris ES, Wyler SC (2012) Serotonergic transcriptional networks and potential importance to mental health. Nat Neurosci 15:519–527.

Drevets WC, Frank E, Price JC, Kupfer DJ, Holt D, Greer PJ, Huang Y, Gautier C, Mathis C (1999) PET imaging of serotonin 1A receptor binding in depression. Biol Psychiatry 46:1375–1387.

Fetsko LA, Xu R, Wang Y (2005) Effects of age and dopamine D2L receptor-deficiency on motor and learning functions. Neurobiol Aging 26:521–530.

Fuxe K, Marcellino D, Leo G, Agnati LF (2010) Molecular integration via allosteric interactions in receptor heteromers: a working hypothesis. Curr Opin Pharmacol 10:14–22.

Garcia-Garcia AL, Meng Q, Canetta S, Gardier AM, Guiard BP, Kellendonk C, Dranovsky A, Leonardo ED (2017) Serotonin signaling through prefrontal cortex 5-HT1A receptors during adolescence can determine baseline mood-related behaviors. Cell Rep 18:1144–1156.

Grace AA (2016) Dysregulation of the dopamine system in the pathophysiology of schizophrenia and depression. Nat Rev Neurosci 17:524–532.

Graybiel AM, Aosaki T, Flaherty AW, Kimura M (1994) The basal ganglia and adaptive motor control. Science 265:1826–1831.

Gutknecht L, Popp S, Waider J, Sommerlandt FM, Göppner C, Post A, Reif A, van den Hove D, Strekalova T, Schmitt A, Colaşo MB, Sommer C, Palme R, Lesch KP (2015) Interaction of brain 5-HT synthesis deficiency, chronic stress and sex differentially impact emotional behavior in Tph2 knockout mice. Psychopharmacology 232:2429–2441.

Hamon M, Gozlan H, el Mestikawy S, Emerit MB, Bolaños F, Schechter L (1990) The central 5-HT1A receptors: pharmacological, biochemical, functional, and regulatory properties. Ann N Y Acad Sci 600:114–129.

Hasegawa E, Yanagisawa M, Sakurai T, Mieda M (2014) Orexin neurons suppress narcolepsy via 2 distinct efferent pathways. J Clin Invest 124:604–616.

Hayden EP, Klein DN, Dougherty LR, Olino TM, Laptook RS, Dyson MW, Bufferd SJ, Durbin CE, Sheikh HI, Singh SM (2010) The dopamine D2 receptor gene and depressive and anxious symptoms in childhood: associations and evidence for gene-environment correlation and gene-environment interaction. Psychiatr Genet 20:304–310.

Heisler LK, Chu HM, Brennan TJ, Danao JA, Bajwa P, Parsons LH, Tecott LH (1998) Elevated anxiety and antidepressant-like responses in serotonin 5-HT1A receptor mutant mice. Proc Natl Acad Sci U S A 95:15049–15054.

Hendricks T, Francis N, Fyodorov D, Deneris ES (1999) The ETS domain factor pet-1 is an early and precise marker of central 5-HT neurons and interacts with a conserved element in serotonergic genes. J Neurosci 19:10348–10356.

Hjorth S, Suchowski CS, Galloway MP (1995) Evidence for 5-HT autoreceptor-mediated, nerve impulse-independent, control of 5-HT synthesis in the rat brain. Synapse 19:170–176.

Hoyer D, Middlemiss DN (1989) Species differences in the pharmacology of terminal 5-HT autoreceptors in mammalian brain. Trends Pharmacol Sci 10:130–132.

Hoyer D, Hannon JP, Martin GR (2002) Molecular, pharmacological and functional diversity of 5-HT receptors. Pharmacol Biochem Behav 71:533–554.

Hranilovic D, Bucan M, Wang Y (2008) Emotional response in dopamine D2L receptor-deficient mice. Behav Brain Res 195:246–250.

Jans LA, Riedel WJ, Markus CR, Blokland A (2007) Serotonergic vulnerability and depression: assumptions, experimental evidence and implications. Mol Psychiatry 12:522–543.

Khan ZU, Mrzljak L, Gutierrez A, de la Calle A, Goldman-Rakic PS (1998) Prominence of the dopamine D2 short isoform in dopaminergic pathways. Proc Natl Acad Sci U S A 95:7731–7736.

Kühhorn J, Götz A, Hübner H, Thompson D, Whistler J, Gmeiner P (2011) Development of a bivalent dopamine D2 receptor agonist. J Med Chem 54:7911–7919.

Kusserow H, Davies B, Hörtnagl H, Voigt I, Stroh T, Bert B, Deng DR, Fink H, Veh RW, Theuring F (2004) Reduced anxiety-related behaviour in transgenic mice overexpressing serotonin 1A receptors. Brain Res Mol Brain Res 129:104–116.

Lawford BR, Young R, Noble EP, Kann B, Ritchie T (2006) The D2 dopamine receptor (DRD2) gene is associated with co-morbid depression, anxiety and social dysfunction in untreated veterans with post-traumatic stress disorder. Eur Psychiatry 21:180–185.

Lemonde S, Turecki G, Bakish D, Du L, Hrdina PD, Bown CD, Sequeira A, Kushwaha N, Morris SJ, Basak A, Ou XM, Albert PR (2003) Impaired repression at a 5-hydroxytryptamine 1A receptor gene polymorphism associated with major depression and suicide. J Neurosci 23:8788–8799.

Lindgren N, Usiello A, Goiny M, Haycock J, Erbs E, Greengard P, Hokfelt T, Borrelli E, Fisone G (2003) Distinct roles of dopamine D2L and D2S receptor isoforms in the regulation of protein phosphorylation at presynaptic and postsynaptic sites. Proc Natl Acad Sci U S A 100:4305–4309.

Łukasiewicz S, Faron-Górecka A, Dobrucki J, Polit A, Dziedzicka-Wasylewska M (2009) Studies on the role of the receptor protein motifs possibly involved in electrostatic interactions on the dopamine D1 and D2 receptor oligomerization. FEBS J 276:760–775.

Łukasiewicz S, Polit A, Kędracka-Krok S, Wędzony K, Maćkowiak M, Dziedzicka-Wasylewska M (2010) Hetero-dimerization of serotonin $5\text{-}HT_{2A}$ and dopamine D_2 receptors. Biochim Biophys Acta 1803:1347–1358.

Łukasiewicz S, Błasiak E, Szafran-Pilch K, Dziedzicka-Wasylewska M (2016) Dopamine D2 and serotonin 5-HT1A receptor interaction in the context of the effects of antipsychotics: *in vitro* studies. J Neurochem 137:549–560.

Muraki Y, Yamanaka A, Tsujino N, Kilduff TS, Goto K, Sakurai T (2004) Serotonergic regulation of the orexin/hypocretin neurons through the $5\text{-}HT_{1A}$ receptor. J Neurosci 24:7159–7166.

Neumeister A, Bain E, Nugent AC, Carson RE, Bonne O, Luckenbaugh DA, Eckelman W, Herscovitch P, Charney DS, Drevets WC (2004) Reduced serotonin type 1A receptor binding in panic disorder. J Neurosci 24:589–591.

Newman-Tancredi A, Kleven MS (2011) Comparative pharmacology of antipsychotics possessing combined dopamine D_2 and serotonin $5\text{-}HT_{1A}$ receptor properties. Psychopharmacology 216:451–473.

Nutt DJ (2008) Relationship of neurotransmitters to the symptoms of major depressive disorder. J Clin Psychiatry 69:4–7.

Parks CL, Robinson PS, Sibille E, Shenk T, Toth M (1998) Increased anxiety of mice lacking the serotonin1A receptor. Proc Natl Acad Sci U S A 95:10734–10739.

Pfaar H, von Holst A, Vogt Weisenhorn DM, Brodski C, Guimera J, Wurst W (2002) mPet-1, a mouse ETS-domain transcription factor, is expressed in central serotonergic neurons. Dev Genes Evol 212:43–46.

Ramboz S, Oosting R, Amara DA, Kung HF, Blier P, Mendelsohn M, Mann JJ, Brunner D, Hen R (1998) Serotonin receptor 1A knockout: an animal model of anxiety-related disorder. Proc Natl Acad Sci U S A 95:14476–14481.

Riad M, Garcia S, Watkins KC, Jodoin N, Doucet E, Langlois X, el Mestikawy S, Hamon M, Descarries L (2000) Somatodendritic localization of 5-HT1A and preterminal axonal localization of 5-HT1B serotonin receptors in adult rat brain. J Comp Neurol 417:181–194.

Richardson-Jones JW, Craige CP, Guiard BP, Stephen A, Metzger KL, Kung HF, Gardier AM, Dranovsky A, David DJ, Beck SG, Hen R, Leonardo ED (2010) 5-HT1A autoreceptor levels determine vulnerability to stress and response to antidepressants. Neuron 65:40–52.

Richardson-Jones JW, Craige CP, Nguyen TH, Kung HF, Gardier AM, Dranovsky A, David DJ, Guiard BP, Beck SG, Hen R, Leonardo ED (2011) Serotonin-1A autoreceptors are necessary and sufficient for the normal formation of circuits underlying innate anxiety. J Neurosci 31:6008–6018.

Schneier FR, Leibowitz MR, Abi-Dargham A, Zea-Ponce Y, Lyn SH, Laurelle M (2000) Low dopamine D_2 receptor binding potential in social phobia. Am J Psychiatry 157:457–459.

Shioda N, Yamamoto Y, Han F, Moriguchi S, Yamaguchi Y, Hino M, Fukunaga K (2010a) A novel cognitive enhancer, ZSET1446/ST101, pro-

motes hippocampal neurogenesis and ameliorates depressive behavior in olfactory bulbectomized mice. J Pharmacol Exp Ther 333:43–50.

Shioda N, Yamamoto Y, Watanabe M, Binas B, Owada Y, Fukunaga K (2010b) Heart-type fatty acid binding protein regulates dopamine D2 receptor function in mouse brain. J Neurosci 30:3146–3155.

Shioda N, Yabuki Y, Wang Y, Uchigashima M, Hikida T, Sasaoka T, Mori H, Watanabe M, Sasahara M, Fukunaga K (2017) Endocytosis following dopamine D2 receptor activation is critical for neuronal activity and dendritic spine formation via rabex-5/PDGFRβ signaling in striatopallidal medium spiny neurons. Mol Psychiatry 22:1205–1222.

Shioda N, Yabuki Y, Yamaguchi K, Onozato M, Li Y, Kurosawa K, Tanabe H, Okamoto N, Era T, Sugiyama H, Wada T, Fukunaga K (2018) Targeting G-quadruplex DNA as cognitive function therapy for ATR-X syndrome. Nat Med 24:802–813.

Sim HR, Choi TY, Lee HJ, Kang EY, Yoon S, Han PL, Choi SY, Baik JH (2013) Role of dopamine D2 receptors in plasticity of stress-induced addictive behaviours. Nat Commun 4:1579.

Söderberg O, Gullberg M, Jarvius M, Ridderstråle K, Leuchowius KJ, Jarvius J, Wester K, Hydbring P, Bahram F, Larsson LG, Landegren U (2006) Direct observation of individual endogenous protein complexes in situ by proximity ligation. Nat Methods 3:995–1000.

Soriano A, Ventura R, Molero A, Hoen R, Casadó V, Cortés A, Fanelli F, Albericio F, Lluís C, Franco R, Royo M (2009) Adenosine A2A receptor-antagonist/dopamine D2 receptor-agonist bivalent ligands as pharmacological tools to detect A2A-D2 receptor heteromers. J Med Chem 52:5590–5602.

Strobel A, Gutknecht L, Rothe C, Reif A, Mössner R, Zeng Y, Brocke B, Lesch KP (2003) Allelic variation in 5-HT1A receptor expression is associated with anxiety- and depression-related personality traits. J Neural Transm 110:1445–1453.

Torres GE, Gainetdinov RR, Caron MG (2003) Plasma membrane monoamine transporters: structure, regulation and function. Nat Rev Neurosci 4:13–25.

Usiello A, Baik JH, Rougé-Pont F, Picetti R, Dierich A, LeMeur M, Piazza PV, Borrelli E (2000) Distinct functions of the two isoforms of dopamine D2 receptors. Nature 408:199–203.

Wang Y, Xu R, Sasaoka T, Tonegawa S, Kung MP, Sankoorikal EB (2000) Dopamine D2 long receptor-deficient mice display alterations in striatum-dependent functions. J Neurosci 20:8305–8314.

Wei GH, Badis G, Berger MF, Kivioja T, Palin K, Enge M, Bonke M, Jolma A, Varjosalo M, Gehrke AR, Yan J, Talukder S, Turunen M, Taipale M, Stunnenberg HG, Ukkonen E, Hughes TR, Bulyk ML, Taipale J (2010) Genome-wide analysis of ETS-family DNA-binding *in vitro* and *in vivo*. EMBO J 29:2147–2160.

Williams JT, Colmers WF, Pan ZZ (1988) Voltage- and ligand-activated inwardly rectifying currents in dorsal raphe neurons *in vitro*. J Neurosci 8:3499–3506.

Wyler SC, Donovan LJ, Yeager M, Deneris E (2015) Pet-1 controls tetrahydrobiopterin pathway and Slc22a3 transporter genes in serotonin neurons. ACS Chem Neurosci 6:1198–1205.

Wyler SC, Spencer WC, Green NH, Rood BD, Crawford L, Craige C, Gresch P, McMahon DG, Beck SG, Deneris E (2016) Pet-1 switches transcriptional targets postnatally to regulate maturation of serotonin neuron excitability. J Neurosci 36:1758–1774.

Xu Y, Piston DW, Johnson CH (1999) A bioluminescence resonance energy transfer (BRET) system: application to interacting circadian clock proteins. Proc Natl Acad Sci U S A 96:151–156.

Yabuki Y, Matsuo K, Izumi H, Haga H, Yoshida T, Wakamori M, Kakei A, Sakimura K, Fukuda T, Fukunaga K (2017) Pharmacological properties of SAK3, a novel T-type voltage-gated Ca^{2+} channel enhancer. Neuropharmacology 117:1–13.

Yamaguchi H, Aiba A, Nakamura K, Nakao K, Sakagami H, Goto K, Kondo H, Katsuki M (1996) Dopamine D2 receptor plays a critical role in cell proliferation and proopiomelanocortin expression in the pituitary. Genes Cells 1:253–268.

Zhang Y, Bertolino A, Fazio L, Blasi G, Rampino A, Romano R, Lee ML, Xiao T, Papp A, Wang D, Sadée W (2007) Polymorphisms in human dopamine D2 receptor gene affect gene expression, splicing, and neuronal activity during working memory. Proc Natl Acad Sci U S A 104:20552–20557.